Journal
American Ceramic Society

Structural origin of the weak germanate anomaly in lead germanate glass properties

Oliver L. G. Alderman[1,†] ◉ | Alex C. Hannon[1] ◉ | Diane Holland[2] | Ray Dupree[2] | Steve Feller[3]

[1] ISIS Neutron and Muon Source, Chilton, Rutherford Appleton Laboratory, Didcot, Oxon, UK

[2] Department of Physics, University of Warwick, Coventry, West Midlands, UK

[3] Department of Physics, Coe College, Cedar Rapids, Iowa, USA

Correspondence
Oliver L. G. Alderman, ISIS Neutron and Muon Source, Rutherford Appleton Laboratory, Chilton, Didcot, Oxon OX11 0QX, UK.
Email: oliver.alderman@stfc.ac.uk and alex.hannon@stfc.ac.uk

[†] Previously affiliated with the Department of Physics, University of Warwick, Coventry, West Midlands, UK.

Abstract

Binary $PbO-GeO_2$ glasses have been studied in detail from 5 to 75 mol% PbO using high-resolution neutron diffraction, high-energy X-ray diffraction, 207-Pb NMR, pycnometry, and thermal analysis. The Ge–O coordination number displays a broad maximum $n_{GeO} = 4.14(3)$ close to 27 mol% PbO. This is smaller than the maximum $n_{GeO} = 4.3$ reported in $CaO-GeO_2$ glasses but occurs at a similar composition. This structural behavior appears to explain the relatively weak germanate anomaly manifest in lead germanate glasses, for example as a maximum in the measured atom number density and a plateau in the glass transition temperatures. The structural role of Pb(II) is complex. On the one hand, short covalent Pb–O bonds and small Pb–O coordination numbers of ∼3 to 4 indicate glass network former character for Pb(II), associated with a stereochemically active electron lone pair. On the other hand, the presence of some GeO_5 or GeO_6 units, in addition to the majority GeO_4 tetrahedral species, indicates some modifier character of Pb(II) at low PbO contents, giving rise to the observed weak germanate anomaly, as well as elongation and enhanced ionicity of the Pb–O bonds. Overall, the observed structural behavior of Pb(II) in lead germanate glasses appears as intermediate between that observed in lead silicate and lead borate glasses. Despite rapid quenching, at low PbO contents, the glasses studied exhibited nanoscale heterogeneity, evidenced by small-angle X-ray scattering consistent with the early stages of spinodal decomposition.

1 | INTRODUCTION

Lead germanate glasses combine desirable optical properties, such as high linear and non-linear refractive indices and visible to mid-infrared (MIR) transmission, with excellent thermal and chemical stability. This synergetic combination of properties has seen $PbO-GeO_2$ based glasses proposed as a practical alternative to MIR tellurite glasses,[1] and they have been investigated for applications including Raman amplifiers,[2] hosts for optically active rare-earths,[3] low loss optical fibers,[1,4–6] and more.[7–9] Accordingly, a wide variety of techniques have been applied to investigate the atomic-scale structure of lead germanate glasses, including Raman,[10–12] 207-Pb nuclear magnetic resonance (NMR),[13] and Ge K-edge[11,13–15] and Pb L_{III}-edge[11,13,16] extended range X-ray absorption fine structure (EXAFS) spectroscopies; molecular dynamics simulations;[14,16–19] and neutron[20,21] and X-ray[19,22,23] diffraction. The literature
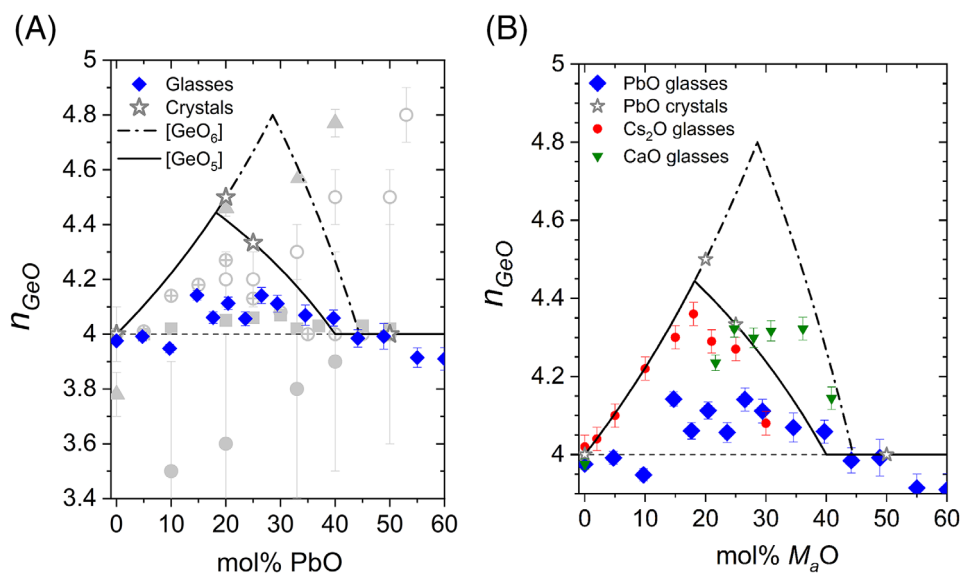
FIGURE 1 Ge–O coordination numbers as a function of PbO–GeO$_2$ glass composition, using neutron diffraction in this study (blue diamonds), extracted by means of integration of $rT^N(r)$ (Table 4). Comparison is made in (A) to values reported in the literature using neutron diffraction[21] (triangles), Ge K-edge EXAFS (circles: filled,[11] open,[14] with crosses[15]) and classical molecular dynamics[17] (squares). Values for crystalline lead germanates[56,57,67,74,75] are also shown (open stars). Curves are the analytical models of Hannon et al.[59] for five (solid) or six (dash–dot) coordinated germanium. In (B) comparison is made to Ge–O coordination numbers from neutron diffraction for vitreous calcium[53] and caesium[55] germanates. In colour online

is more or less consistent in revealing that Pb^{2+} forms short bonds to oxygen and has low coordination numbers of 3 to 4. In this respect, Pb^{2+} acts like an oxide glass-network-forming cation, as opposed to a typical network modifier such as Ca^{2+}. On the other hand, there is disagreement within the literature regarding the (average) coordination states of Ge^{4+}. The lack of consensus is illustrated in Figure 1A which reveals both quantitative and qualitative differences between reports of the average Ge–O coordination numbers, n_{GeO}. As the PbO content of the glasses is increased, some studies find that n_{GeO} rises with it in a continuous manner, while others find that it passes through a maximum.

Germanate glasses are considered anomalous, as compared with analogous silicates, on account of the fact that their physical properties often demonstrate extrema as a function of composition. This behavior, coined the "germanate anomaly," is strongly linked with the average Ge–O coordination number which can often take values greater than four, unlike in silicates where the glass and crystalline networks are usually composed largely of SiO$_4$ tetrahedra. Examples of physical property extrema in lead germanate glasses include those in the optical band gap and absorption edge,[24] a maximum in atom number density (Figure 2) and resistivity,[25] and in the Young's and shear moduli[26] at ~30 mol% PbO.

The present paper addresses the stated inconsistencies within the literature by measuring accurately the behavior of n_{GeO} as a function of PbO content. In order to achieve

this, 18 glasses containing from 5 to 75 mol% PbO were studied using high-resolution neutron diffraction, supported by high-energy X-ray diffraction, 207-Pb NMR, X-ray spectroscopy, pycnometry, and thermal analysis.

2 | EXPERIMENTAL

2.1 | Glass preparation

Two series of lead germanate, xPbO(100 − x)GeO$_2$, glasses were produced. The first consisted of 15 compositions with $5 \leq x \leq 65$ mol% PbO, prepared by mixing quartz GeO$_2$ (Alfa Aesar, 99.98%) and Pb$_3$O$_4$ (Aldrich, 99%) in sufficient quantities to yield 20 g of glass. The mixed-valence compound lead (II, IV) oxide was used, rather than divalent lead (II) oxide (PbO), in order to provide additional oxygen to suppress the reduction of any part of the melt to metallic Pb. Instead, the reduction of the tetravalent Pb to the divalent form, and evolution of oxygen gas occurs at 500°C.[27] The two powders were well mixed and placed into 90Pt.10Rh crucibles inside an electric furnace at room temperature, under an air atmosphere. The furnace temperature was increased at a rate of 600°C/h typically until 1000°C, and then held for 25 min. The liquids thus obtained were quenched by pouring them onto a steel plate and quickly pressing their upper surface with a brass plate to provide rapid quenching, of the order 10^3 °C/s and to yield a thin (≈1 mm thick) glass disk.
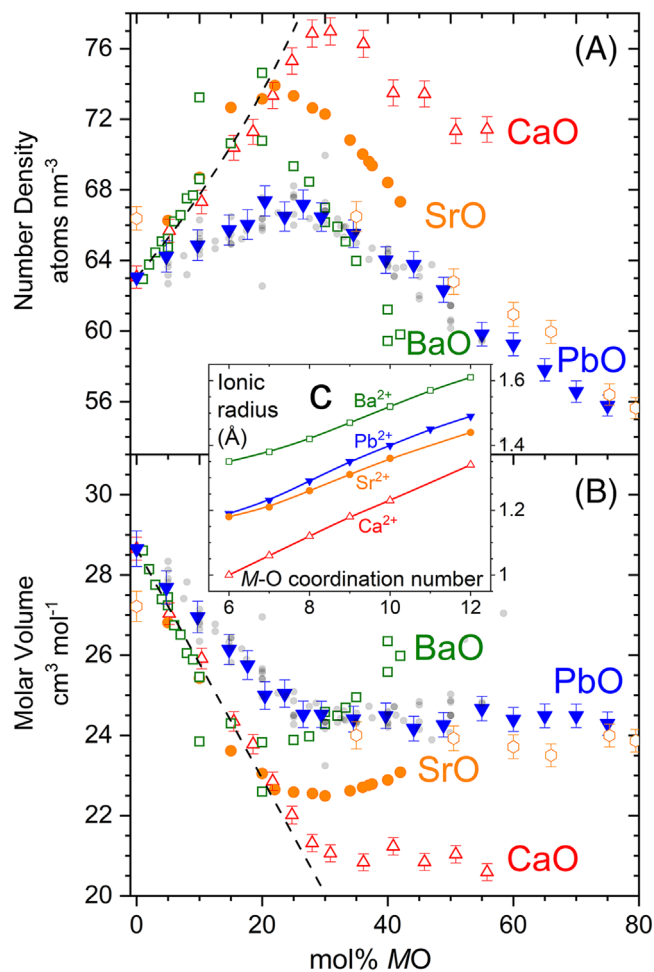
FIGURE 2 (A) Atom number densities and (B) molar volumes of PbO–GeO$_2$ glasses measured in this study (blue triangles, Table 1), compared to data from the SciGlass database[47] (grey circles), references therein. Also shown are equivalent data for binary calcium[53] (open red triangles), strontium[76] (orange circles) and barium[76–79] (green open squares) germanate glasses and lead silicate[38,49] glasses (open orange hexagons). The dashed curves are those of constant volume per mole $JMO.GeO_2$, equivalent to constant Ge atom partial number density. (C) Inset are the M^{2+} Shannon–Prewitt ionic radii[65] as functions of M–O coordination number from 6 to 12. In colour online

and not of GeO$_2$, are recorded in Table 1. However, in several cases, this was not possible owing to the violent fracture of the glass plates obtained, which occurs due to cooling rate differences between the glass surface and its interior, and associated high stresses. This often led to the loss of small glass fragments, rendering calculation of the correct PbO content from the mass loss impracticable. In these cases (15, 18, 24, 27 mol% PbO) the PbO content was adjusted by linear interpolation using the successful measurements.

The highest Pb content compositions, with $55 \leq x \leq 65$ mol% PbO, all contained visible crystalline fractions after quenching, this being extensive in the 65 mol% PbO case and very minor in the 55 mol% PbO case. In the former, laboratory X-ray diffraction confirmed the presence of Pb$_5$Ge$_3$O$_{11}$[28,29] and Pb$_3$GeO$_5$.[30]

In an attempt to obtain high Pb glasses, free from crystalline inclusions, a second series of glasses was produced using smaller batch sizes and more rapid, twin-roller, quenching. Batches of quartz GeO$_2$ (Alfa Aesar, 99.98%) and Pb$_3$O$_4$ (Sigma-Aldrich, 99%) were mixed in sufficient quantities to yield 10 g of germanate glass, containing $55 \leq x \leq 75$ mol% PbO, in 5 mol% PbO intervals. These were held in 20 cm^3 platinum crucibles and placed inside an electric furnace held at a constant temperature of 900°C for 20 min. The resultant melts were quenched by pouring into a 30 μm gap between two steel cylinders counter-rotating at 590 rpm, resulting in a cooling rate of order 10^5°C/s.[31] While the 55 and 60 mol% PbO samples appeared completely amorphous, the higher Pb content samples contained some crystalline features, and these included metallic Pb in the 75 mol% PbO glass. In order to avoid damage to the Pt crucibles by alloying with metallic Pb, batches with > 75 mol% PbO were not melted. Two batches of each glass composition were produced, and those containing the least inclusions were chosen for further study, with inclusions removed.

2.2 | Density measurement

Sample volumes were measured by helium pycnometry in a Micromeritics Accupyc 1330 pycnometer, and combined with the sample mass to give the mass densities, ρ_m. Calibration was performed prior to each set of measurements using steel spheres of certified volume. Furthermore, measurements of a silica glass rod standard were made periodically to check for drift. The ρ_m obtained were used to derive molar volumes, V_M, and atomic number densities, ρ_0.

2.3 | Energy-dispersive X-ray spectroscopy

Glass composition was measured using energy-dispersive X-ray spectroscopy (EDX) in a Zeiss SUPRA 55-VP field

The following exceptions to the above apply. Glasses containing $55 \leq x \leq 65$ mol% PbO were held at 900°C, whilst the 15 mol% PbO germanate glass was held at 1100°C and the 5 and 10 mol% PbO glasses at 1200°C. Despite the higher melt temperature, the latter two melt compositions were too viscous to allow pouring and were therefore quenched by placing the base of the crucible into cold tap water.

Mass loss measurements were made in order to check that all the additional oxygen associated with Pb(IV) had evolved, and for the possibility of volatilization. In most cases, additional mass loss, in excess of that expected due to evolution of oxygen gas, was recorded, and the glass compositions estimated assuming volatilization only of PbO,

TABLE 1 Measured mass (ρ_m) and number (ρ_0) densities, molar volumes (V_M), glass transition temperatures (T_g) and compositions for lead germanate glasses. Uncertainties in parentheses. Compositions were derived either from the measured mass loss during melting, assuming preferential volatilisation of PbO, or by energy dispersive X-ray (EDX) spectroscopy. The former will be used in subsequent Tables

Glass composition in mol% PbO			ρ_m	ρ_0	V_M	T_g
Nominal	Mass loss[†]	EDX	g cm^{-3}	atoms nm^{-3}	cm^3 mol^{-1}	± 5°C
Plate quenched glasses						
0[§]	–	–	3.65(2)	63.0(3)	28.7(1)	526(27)
5	4.74(5)	6.2(1)	3.98(4)	64.2(9)	27.7(4)	467
10	9.72(5)	11.0(1)	4.31(4)	64.9(9)	27.0(4)	455
15	14.73(5)[‡]	16.0(2)	4.67(5)	65.7(9)	26.1(4)	454
18	17.68(5)[‡]	18.8(2)	4.88(5)	66.0(8)	25.7(4)	456
21	20.42(5)	18.7(7)	5.15(5)	67.4(9)	25.0(3)	459
24	23.57(5)[‡]	22.1(5)	5.29(5)	66.5(8)	25.0(3)	455
27	26.51(5)[‡]	26.7(3)	5.55(6)	67.2(8)	24.5(3)	452
30	29.42(5)	29.5(8)	5.69(6)	66.5(8)	24.5(3)	445
35	34.54(5)	34.6(4)	5.96(6)	65.5(8)	24.4(3)	427
40	39.69(5)	38.3(3)	6.19(6)	64.0(7)	24.5(3)	410
45	44.13(5)	43.7(5)	6.49(6)	63.8(7)	24.2(3)	387
50	48.88(5)	47.7(2)	6.70(7)	62.3(7)	24.3(3)	377
55[*]	54.75(5)	52.7(5)	6.98(7)	60.8(7)	24.3(3)	–
60[*]	59.81(5)	57.0(7)	7.35(7)	60.6(7)	23.9(3)	–
65[*]	64.78(5)	62.3(5)	7.63(8)	59.6(7)	23.8(3)	–
Twin-roller quenched glasses						
55	–	56.1(4)	6.89(7)	59.8(7)	24.7(3)	348
60	–	60.8(8)	7.20(7)	59.2(7)	24.4(3)	331
65	–	66(1)	7.42(7)	57.8(6)	24.5(3)	326
70	–	71.0(9)	7.66(8)	56.6(6)	24.5(3)	319
75	–	75.1(8)	7.97(8)	55.8(6)	24.3(3)	309

[†]Assuming preferential volatilisation of PbO.
[‡]Interpolated.
*Partial crystallisation.
[§]Values for GeO$_2$ are averages over literature data collated within the SciGlass database,[47] outliers excluded.

emission gun scanning electron microscope (FEGSEM) operating at an accelerating voltage of 20 kV. Samples were mounted on aluminum stubs using an organic silver paste, and carbon-coated using a vacuum evaporator to provide conduction pathways and avoid surface charging of the glass. EDX spectra were collected over 100 s exposure times at various points on the surface of a number of different glass pieces. Quantification of the glass composition was based on the integrated intensities of the Pb L and Ge K lines of the spectra after background subtraction and ZAF corrections for atomic number (Z) dependent electron backscatter and stopping power, absorption (A), and fluorescence (F), using the EDAX Genesis software, which employs internal standards.

2.4 | Differential thermal analysis

Differential thermal analysis (DTA) was performed using 100 mg of powdered glass sample and 100 mg of Al$_2$O$_3$ reference powder heated in Pt/Rh crucibles from room temperature to above the sample melting points at a rate of 10°C min^{-1}. Although all exothermic crystallization events and endothermic melting events were recorded, here only the glass transition temperatures, T_g, are quoted, as a means of sample characterization, for comparison to values in the literature, and for tracking changes in T_g as a function of glass composition, which can be related to structural changes in the glasses/supercooled melts. T_g was taken as the intersection of linear extrapolations of the data at temperatures below the heat capacity step, and of the slope of the step itself.

2.5 | 207-Pb nuclear magnetic resonance

207-Pb static NMR spectra were acquired using a field-step method (described previously[32]) in order to provide uniform irradiation of the broad spectral envelopes. A primary field of 7.05 T and operating frequencies of

62.36 to 62.43 MHz were used in pulse-echo ($\pi/2 \rightarrow \pi$) experiments with $\tau/2 = 3\,\mu s$, $\tau = 6\,\mu s$, 2 to 8 s pulse delays and 500 kHz spectral width at each step. 960 to 1536 acquisitions were made at each of 28 or 31 steps of 22.72 kHz, resulting in total spectral widths in excess of 1.1 MHz. Spectra are referenced to tetramethyl lead at 0 ppm, using polycrystalline β-PbO as a secondary reference ($\delta_{iso} = 1515$ ppm[33]).

2.6 | Neutron diffraction

Time-of-flight neutron diffraction measurements were made using the GEneral Materials (GEM)[34] diffractometer at the ISIS Facility, Rutherford Appleton Laboratory, UK. The plate quenched glasses, containing $5 \leq x \leq 50$ mol% PbO, were broken into small (mm sized) pieces, and placed within thin-walled, 8.3 mm diameter, vanadium containers. On account of the lesser amount of material available, the roller quenched glasses, containing $55 \leq x \leq 75$ mol% PbO, were placed inside 5 mm diameter vanadium containers. These latter glasses, in the smaller containers, were exposed to the neutron beam for a factor of 1.76 longer than the plate quenched glasses in the larger containers. A maximum momentum transfer $Q_{max} = 40.0$ Å^{-1} was used for Fourier transformation. Measurements were also performed on an empty vanadium container, the empty instrument, and an 8.34 mm diameter vanadium rod for normalization purposes and to allow for the subtraction of background signals. A vitreous germania sample was also measured.[20]

2.7 | X-ray diffraction

Wiggler beamline (BW5)[35,36] on the synchrotron radiation source DORIS III, HASYLAB at DESY, was used for X-ray diffraction measurements of the powdered glasses, which were held inside 1.5 mm diameter silica glass capillaries (10 μm wall thickness). Measurements of an empty capillary and the empty instrument were made to allow the removal of background scattering. X-ray energies of 85.336 and 84.768 keV were used for low ($\leq$ 50 mol%) and high (> 50 mol%) PbO glasses respectively, so as to minimize the photoelectric absorption cross-section whilst avoiding fluorescence associated with the Pb K-edge at 88.0045 keV,[37] and making accessible large maximum momentum transfers, $Q_{max} = 4\pi \sin(\theta_{max})/\lambda = 23.78$ Å^{-1} and 23.62 Å^{-1} respectively, at the maximum scattering angle of $2\theta_{max} = 32.0°$. Data were collected in three angular ranges using different attenuators between sample and detector, owing to the form factor dependence of X-ray signal, and to ensure that the count rate in the Ge detector did not saturate. All sets of data were combined after omission of bad points, dead-time correction, normalization to the incident beam monitor counts, correction for the geometrical arrangement of the detector and sample and scaling as required for datasets for which different levels of in-beam attenuation were used. A vitreous germania sample was also measured.[20]

2.8 | Total scattering formalism

Herein the same definitions of the real- and reciprocal-space scattering functions are used as in our previous work.[38] The real-space total correlation function is defined by

$$T^R(r) = T^{R,0}(r) + \frac{2}{\pi} \int_0^\infty Q i^R(Q) M(Q) \sin(rQ) dQ \quad (1)$$

where $R = N$ or X denotes the radiation type, $i^N(Q)$ is the measured distinct[39] neutron scattering, whereas

$$i^X(Q) = \frac{i(Q)}{\left(\sum_{i=1}^n c_i f_i(Q)\right)^2} \quad (2)$$

is the measured distinct X-ray scattering after division by a sharpening[40] function used to approximately eliminate the X-ray form factor ($f_i(Q)$[41]) Q-dependence of the scattering. Subscripts i denote elements of the periodic table and c_i are atomic fractions. In Equation (1) $M(Q)$ is a modification function which can be chosen to reduce the effects of the finite limits ($0 \lesssim Q \leq Q_{max}$) of the integral which are used in practice. In this study, the $M(Q)$ due to Lorch[42] is chosen. The $T^{R,0}(r)$ represent average scattering density terms and are given by

$$T^{N,0}(r) = 4\pi\rho_0 r \left(\sum_{i=1}^n c_i \bar{b}_i\right)^2 \quad \text{and} \quad T^{X,0}(r) = 4\pi\rho_0 r \quad (3)$$

where bound coherent neutron scattering lengths[43] are denoted $\bar{b}_i$. The $i^R(Q)$ may be written as sums of Faber–Ziman[44] partial structure factors, $S_{ij}(Q)$, and the $T^R(r)$ as sums of partial pair correlation functions, $t_{ij}(r) = 4\pi r c_j \rho_0 g_{ij}(r)$, with $g_{ij}(r)$ the standard pair distribution functions.[39,45] In the neutron case

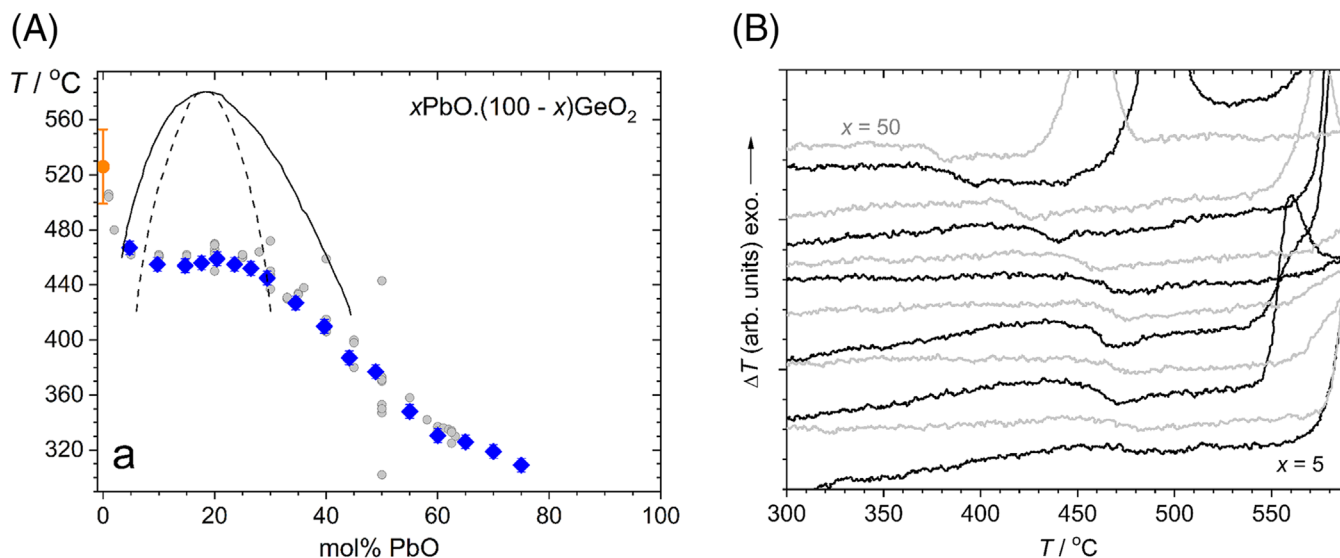$$t_{ij}(r) = \frac{c_j T^N(r)}{(2 - \delta_{ij}) W_{ij}^N} \quad (4)$$

(A)

(B)

FIGURE 3 (A) Lead germanate glass transition temperatures as a function of composition (blue diamonds) compared to literature data obtained from the SciGlass database[47] (grey circles), including the mean value for GeO_2 (orange circle, with standard deviation as error bar). Also shown are the metastable binodal (continuous) and calculated spinodal (dashed) decomposition curves from Morinaga and Nakashima.[49] (B) Portions of the DTA traces illustrating the glass transition features, as well as the lack of a second glass transition in the region of 540°C (as reported by Shelby[46]). Vertical offsets have been applied for clarity, ascending from 5 to 50 mol% PbO with the coloring of the traces alternated between black and gray

over any regions of r to which only a single pair term contributes to the total $T^N(r)$. δ_{ij} is the Kronecker delta and $W_{ij}^N = c_i c_j b_i b_j$.

3 | RESULTS

3.1 | Physical properties

Mass and number densities and molar volumes of PbO–GeO_2 glasses are recorded in Table 1 and plotted for comparison with literature data in Figure 2. There are some notable differences in the compositional trends as compared with the equivalent data for PbO–SiO_2 glasses. While the mass density always increases with PbO content due to the dominance of the mass of the PbO component, an inflection is apparent at ≈27 mol% PbO, and this manifests as a maximum in the atom number densities of the glasses at the same composition. Meanwhile, the behavior of the molar volume is similar to that of the lead silicates, at first decreasing as PbO is added, and then remaining approximately constant from ≈27 mol% PbO onwards.

EDX measurements of the glass compositions based on the Pb L and Ge K lines of the spectra are presented in Table 1. For the plate quenched glasses containing > 20 mol% PbO, these are qualitatively in accord with the mass loss measurements and the assumption of preferential volatilization of PbO from the melt. On the other hand, EDX measurements indicate that the glasses con-

taining < 20 mol% PbO are lead rich with respect to nominal compositions. This implies that GeO_2 is preferentially volatilized from the melt in this composition region, and at the higher melt temperatures used for the 5, 10 and 15 mol% PbO samples. Calculating the glass composition based on loss of GeO_2 gives 10.07(5) mol% PbO, for example, in the case of the nominally 10 mol% PbO composition. Note that although the mass loss from the roller quenched batches was not measured, these were expected to be smaller based on smaller melt surface area to volume ratios, which is supported by the EDX measurements.

Glass transition temperatures measured by DTA are displayed in Table 1 and Figure 3. As noted by Shelby[46] there is a sharp decrease in glass transition temperature upon initial addition of PbO, from that of pure GeO_2 glass at 526(27)°C (mean, with standard deviation in parentheses, of entries in the SciGlass database[47]). This is similar to observations in sodium and caesium germanate glasses.[48]

Following this initial sharp decrease, the transition temperatures plateau between 10 and ≈27 mol% PbO, and it was this feature, along with the detection of a second glass transition, by DSC, at ≈540°C that led Shelby[46] to conclude that his glasses were phase separated. Note however that the DTA measurements collected herein showed no hint of a second glass transition close to 540°C. The absence of a second T_g event near 540°C is quite clear for the nominally 5, 10, 18, 24, 27, 30, and 35 mol% PbO glasses in Figure 3B. The 15 and 21 mol% PbO germanate
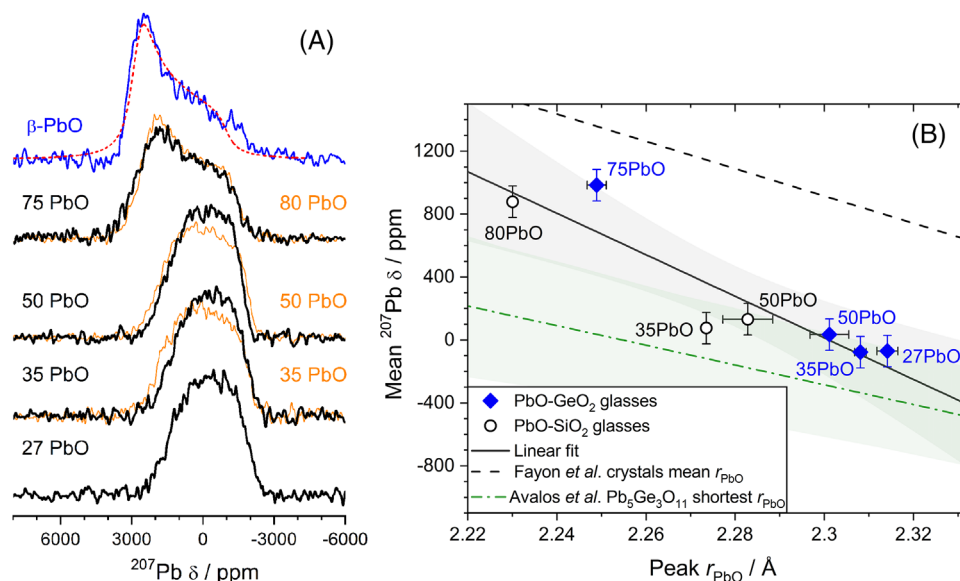
FIGURE 4 (A) Static 207-Pb NMR spectra for four lead germanate glasses (thick black lines) compared to those for lead silicate glasses[51] of similar composition (thin orange lines) and for β-PbO. The suitably broadened simulation of the static CSA lineshape for polycrystalline β-PbO is overlaid on the measured spectrum (dashed line), based on parameters reported by Fayon et al.[33] The slight excess intensity near −1500 ppm in the experimental spectrum from β-PbO is due to the presence of some basic lead carbonate impurity in the sample. Vertical offsets have been applied for clarity. (B) First moments of the 207-Pb NMR lineshapes as a function of peak Pb–O bond length measured by neutron diffraction. Molar compositions are indicated. The solid line is a least-squares fit to the data: $\delta(207\text{-Pb}) = -13200\, r_{PbO}(\text{peak}) + 30380$, in ppm and Å, with 95% confidence bounds shaded. The dashed line is given by Fayon et al.,[33] $\delta(207\text{-Pb}) = -8668.95\, r_{PbO} + 20854$. The main reason for the offset between the two trend lines is attributed to the use of peak (modal) bond lengths herein, which are more easily determined from total scattering data than mean bond lengths, and hence a more reliable indicator of the local environment. The Fayon et al.,[33] correlation is based on mean bond lengths from crystal structures, not from total scattering. The dash–dot line is the correlation derived by Avalos et al.[80] for the *shortest* Pb–O bond lengths of each of the 9 Pb sites in crystalline $Pb_5Ge_3O_{11}$, with 95% confidence bounds shaded. In colour online

glasses begin to show an exothermic release of energy as a result of crystallization very close to 540°C, which could obscure a second glass transition (if present) in these two glasses, although given the lack of such in neighboring compositions, this is thought unlikely. The main difference between the glasses of our study and those of Shelby arises from the different cooling rates, the present glasses having been rapidly plate quenched, while Shelby's glasses were subject to relatively slow cooling rates during vitrification, as well as subsequent annealing, both of which provide more time for the growth of phase-separated domains. Nonetheless, some degree of heterogeneity can be expected in our glasses based on the spinodal line calculated by Morinaga and Nakashima[49] which exceeds the glass transition temperatures between approximately 7 and 29 mol% PbO, see Figure 3A. As discussed below, our X-ray scattering measurements do reveal the presence of some degree of nanoscale heterogeneity in the glass structure, evidenced by the scattered intensity at small angles.

The decline of the glass transition temperature with the subsequent addition of PbO, beyond 27 mol% PbO, is similar to that observed in lead silicate glasses,[50] albeit that the latter are offset to higher temperatures.

3.1.1 | 207-Pb NMR

Static 207-Pb NMR spectra are shown in Figure 4A, and at first glance show great similarity to those for equivalent lead silicate glasses.[51] In both cases, at the highest PbO contents studied, the lineshape shows pronounced asymmetry, consistent with an increased Pb site axial symmetry as compared to the lower PbO content glasses. There are also subtle differences between spectra for germanate and silicate glasses. The first moments of the spectra are recorded in Table 2 and Figure 4B. Chemical shift tensor components, δ_{11}, δ_{22}, and δ_{33}, were obtained by fitting the NMR peaks with static chemical shift anisotropy (CSA) lineshapes.[52] The peaks are then characterized by the derived CSA parameters: isotropic shift, $\delta_{iso} = (\delta_{11} + \delta_{22} + \delta_{33})/3$; span, $\Omega = \delta_{11} - \delta_{33}$; and skew, $\kappa = 3(\delta_{22} - \delta_{iso})/\Omega$; for axial symmetry $\delta_{11} = \delta_{22} \neq \delta_{33}$ and $\kappa = \pm 1$. The distribution of Pb environments in glass means that the lineshape used in fitting should be simulated using distributions of the CSA parameters (or chemical shift tensors). Fitting with single-valued parameters, as herein, leads to significant uncertainties since the distributions cannot be accommodated by the broadening function which is applied

TABLE 2 207-Pb NMR peak fit parameters. Chemical shift components in ppm with respect to tetramethyl lead. Also shown are the first moment "centre-of-gravity" values for isotropic chemical shift, obtained by integration of the experimental spectra. Uncertainties are approximately $\pm$ 50 ppm, or $\pm$ 0.1 for the skew, κ

| mol% PbO	δ_{11} (ppm)	δ_{22} (ppm)	δ_{33} (ppm)	δ_{iso} fit (ppm)	δ_{iso} 1st moment (ppm)	Ω (ppm)	κ
Lead germanate glasses							
26.5	1690	−330	−1970	−200	−70	3660	−0.1
34.5	1630	−370	−1890	−210	−80	3520	−0.1
48.9	1850	−240	−1690	−30	40	3540	−0.2
75	3070	1620	−1580	1030	980	4650	0.4
Lead silicate glasses							
35	2110	35	−1990	50	80	4110	−0.01
50	2110	70	−1950	80	130	4060	0.00
80	2570	1925	−1650	950	880	4220	0.69
Polycrystalline PbO							
β-PbO	3165	2550	−1780	1310	1210	5020	0.75
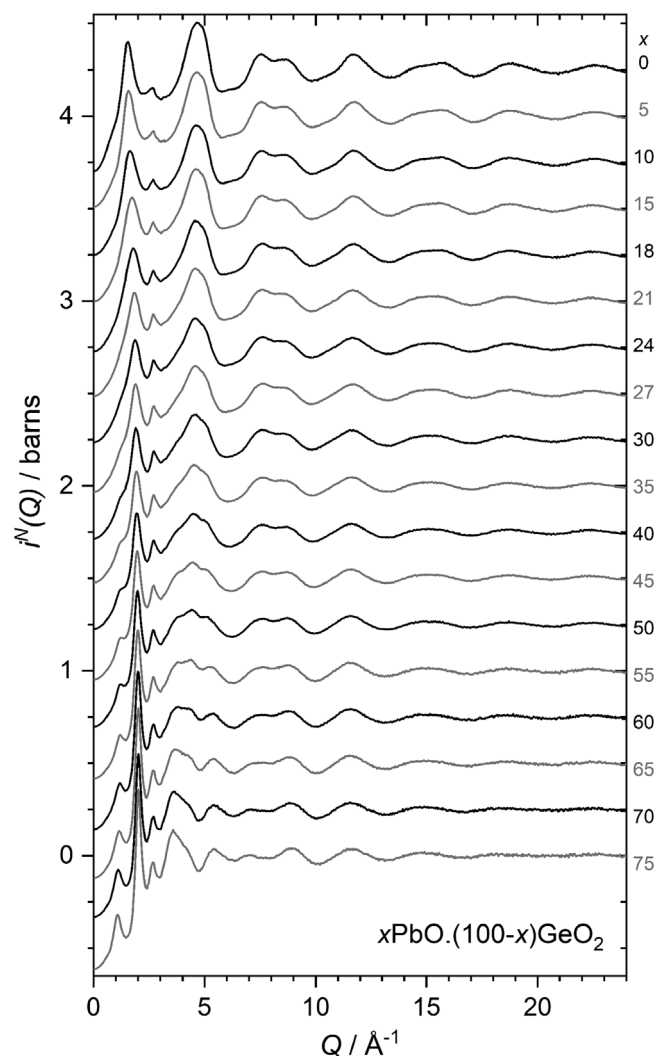
FIGURE 5 Neutron distinct scattering from lead germanate glasses, compared to that for vitreous germania. Molar compositions (nominal) are indicated and vertical offsets have been used for clarity

to achieve a fit. This is particularly obvious for the low PbO samples, where the lineshapes cannot adequately be approximated by any single, broadened line. Table 2 gives the parameters which have been extracted.

3.1.2 | Diffraction

Data reduction procedures were conducted as described previously,[38,53] and the resultant neutron distinct scattering, $i^N(Q)$, is shown in Figure 5, and the X-ray interference functions, $Qi^X(Q)$, are displayed in Figure 6 (numerical data are available as Supporting Information). Note that the regions of $i^N(Q)$ (Figure 5) below 0.45 Å^{-1} were extrapolated by the fitting of a function of form $A + BQ^2$ to the low Q scattering data between $0.45 \le Q \le 0.7$ Å^{-1}. Evidence of small-angle X-ray scattering (SAXS) is evident in the low $Q < 1.3$ Å^{-1} region of $i^X(Q)$, Figure 7. The low Q regions of both $i^X(Q)$ and $i^N(Q)$ from the germanate glasses are qualitatively similar to those of the lead silicates,[38,51] particularly for the high Pb ($\ge$ 50 mol% PbO) glasses, showing a first sharp diffraction peak (FSDP) at $\approx$ 2.0 Å^{-1} and a neutron diffraction pre-peak developing at 1.2 Å^{-1} at $\approx$45 mol% PbO and above. Notably, this pre-peak feature is not resolved until 60 mol% PbO in the diffraction patterns from lead silicate glasses. Details of the low Q diffraction peaks, extracted by fitting of Lorentzian lineshapes to their leading edges, are summarized in Table 3, and the periodicities, $2\pi/Q$, and correlation lengths, $2\pi/\Delta Q$, plotted in Figure 8 where they are compared to the equivalent values from lead silicate glasses.[38,51] The most marked difference compared to the silicates is in the smaller widths, ΔQ, indicative of a more well-developed intermediate-range order. At low PbO contents (< 50 mol% PbO) there is a rise in SAXS apparent at the lowest Q values measured
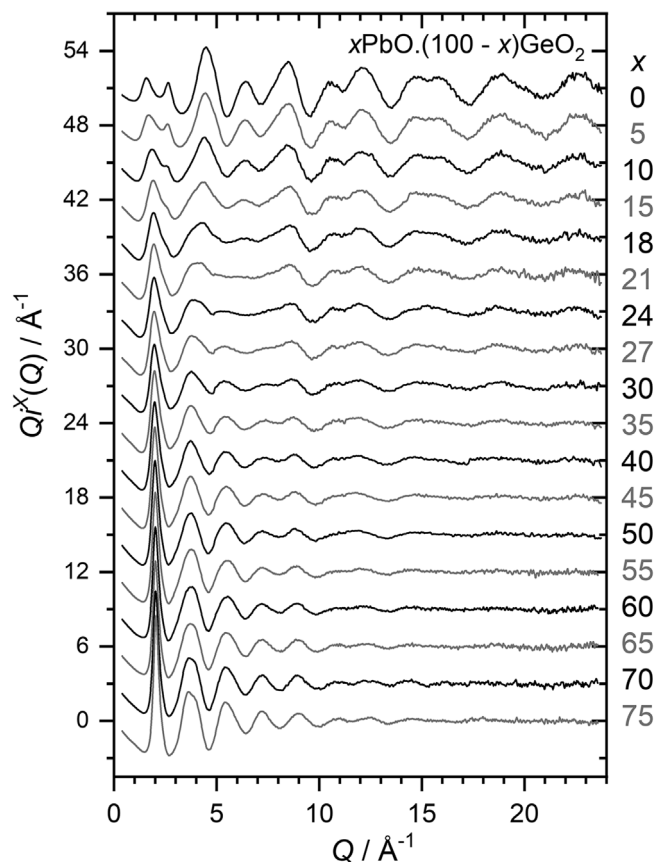
FIGURE 6 X-ray interference functions for lead germanate glasses, compared to that for vitreous germania. Molar compositions (nominal) are indicated and vertical offsets have been used for clarity
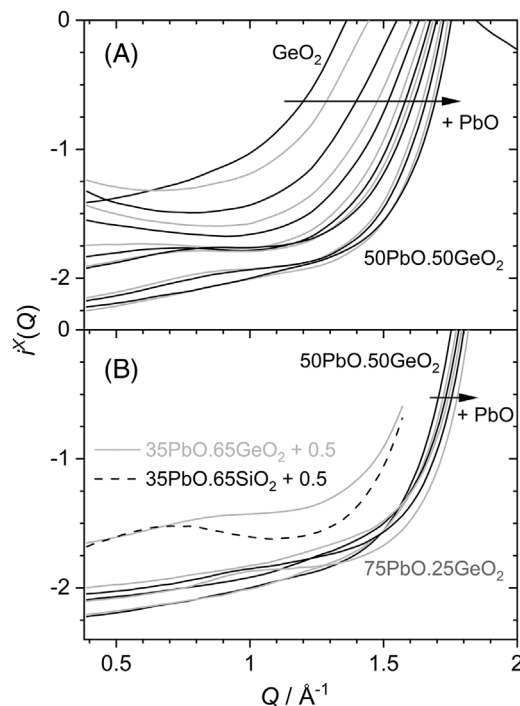

FIGURE 7 Low Q X-ray distinct scattering from lead germanate glasses. Glasses containing (A) 0 to 50 mol% PbO; (B) 50 to 75 mol% PbO, and comparison of $35PbO.65GeO_2$ to $35PbO.65SiO_2$ glass,[51] offset for clarity

(0.45 Å^{-1}) for 5 to 18 mol% PbO germanate glasses. This shifts to higher Q with PbO addition, implying an inhomogeneous incorporation of PbO into the germanate network, on length scales initially above 1 nm, and subsequently below 1 nm from 24 mol% PbO upwards, until no longer apparent at 50 mol% PbO. Based on earlier studies,[25,46] this is likely a pre-cursor to phase-separation occurring on longer length scales after heat treatment, or slower initial cooling of the glasses, and corresponds to the early stages of spinodal decomposition.[49]

Fourier transformation of the interference functions, $Qi^R(Q)$, obtained with large Q_{max} and Lorch[42] modification, resulted in the total correlation functions displayed in Figures 9 and 10 (numerical data are available as Supporting Information). In order to ensure the correct low r behavior of $T^N(r)$ (oscillation about zero, with no slope), a renormalization was applied to $i^N(Q)$ prior to transformation. Renormalization factors were obtained by dividing $T^{N,0}(r)/r$ by the modulus of the low r slope of the differential correlation function, $D^N(r)$, obtained prior to renormalization, which itself was obtained by fitting $D^N(r)$ at low r, including part or all of the Ge–O peak at ≈ 1.75 Å.

These factors account for uncertainties in the measured glass densities and compositions, as well as discrepancies in the normalization of the diffraction data, but typically deviated from unity by no more than 7%.

A key observation is that a peak in $T^N(r)$ (Figure 9) at ≈ 2.3 Å is present for all of the lead germanate glasses, even at 5 mol% PbO. These peaks can be assigned to the Pb–O pair term, and such short Pb–O bonds are typical of Pb^{2+} sites with low coordination numbers and non-bonding electron lone pairs with p-character that are stereochemically active. This implies that at least some of the lead, in all glasses, are playing network forming roles (low oxygen coordination numbers) rather than acting as typical network modifying cations with higher coordination numbers to oxygen.

At high PbO content, the $T^X(r)$ (Figure 10) are dominated by the Pb–Pb term and are highly similar to those of high lead silicate glasses.[38,51] At low PbO content it is interesting to note that a peak at ≈ 3.75 Å appears immediately upon addition of PbO to germania, between the Ge–Ge peak at ≈ 3.17 Å and the second Ge–O peak at 4.45 Å. This is coincident with the position of the first Pb–Pb peak at high PbO content, but in the low PbO region must be ascribed to the Pb–Ge term based on the pair weighting factors (Equation (3)). This implies a most probable Ge–O–Pb bond angle of $\approx 135°$, larger than the Pb–O–Pb angle of $\approx 109°$ but close to the Ge–O–Ge angle of $\sim 130°$.[54]

TABLE 3 Values obtained by fitting of Lorentzian lineshapes to the FSDPs of the X-ray and neutron distinct scattering, and to the pre-peak of the neutron distinct scattering

| mol% PbO	Peak position Q, Å^{-1}	Peak width ΔQ, Å^{-1}	Periodicity $2\pi/Q$, Å	Correlation Length $2\pi/\Delta Q$, Å	Number of periods $Q/\Delta Q$
Pre-peak (ND)					
44.1	1.25(1)	0.78(2)	5.01(4)	8.0(2)	1.60(5)
48.9	1.24(1)	0.76(2)	5.05(4)	8.2(2)	1.63(6)
55	1.22(1)	0.71(1)	5.14(4)	8.9(2)	1.73(5)
60	1.20(1)	0.75(2)	5.22(4)	8.3(2)	1.60(5)
65	1.17(1)	0.68(1)	5.38(5)	9.2(2)	1.72(5)
70	1.12(1)	0.59(1)	5.63(5)	10.6(3)	1.88(6)
75	1.09(1)	0.52(1)	5.78(5)	12.0(3)	2.08(8)
FSDP (ND)					
0	1.54(1)	0.69(1)	4.08(3)	9.1(2)	2.23(6)
4.7	1.58(1)	0.78(2)	3.97(3)	8.1(2)	2.03(5)
9.7	1.64(1)	0.92(1)	3.83(2)	6.8(1)	1.78(4)
14.7	1.73(1)	1.13(1)	3.63(2)	5.6(1)	1.54(3)
17.7	1.79(1)	1.03(3)	3.51(2)	6.1(2)	1.73(5)
20.4	1.84(1)	0.78(1)	3.41(2)	8.1(1)	2.36(6)
23.6	1.87(1)	0.70(1)	3.35(2)	9.0(2)	2.67(7)
26.5	1.89(1)	0.62(1)	3.32(2)	10.2(2)	3.07(9)
29.4	1.91(1)	0.57(1)	3.29(2)	11.1(3)	3.4(1)
34.5	1.93(1)	0.54(1)	3.25(2)	11.7(3)	3.6(1)
39.7	1.95(1)	0.49(1)	3.22(2)	12.8(4)	4.0(1)
44.1	1.97(1)	0.43(1)	3.19(2)	14.7(5)	4.6(2)
48.9	1.98(1)	0.40(1)	3.18(2)	15.8(6)	5.0(2)
55	1.99(1)	0.39(1)	3.15(2)	16.1(6)	5.1(2)
60	2.00(1)	0.37(1)	3.14(2)	17.1(7)	5.5(2)
65	2.01(1)	0.34(1)	3.13(2)	18.3(8)	5.9(3)
70	2.01(1)	0.33(1)	3.12(2)	19.2(8)	6.1(3)
75	2.02(1)	0.32(1)	3.11(2)	19.9(9)	6.4(3)
FSDP (XRD)					
0	1.56(1)	0.65(1)	4.03(3)	9.6(2)	2.39(7)
4.7	1.66(1)	0.75(2)	3.80(2)	8.4(2)	2.21(7)
9.7	1.82(1)	1.01(3)	3.46(2)	6.2(2)	1.79(6)
14.7	1.88(1)	0.86(2)	3.35(2)	7.3(1)	2.17(5)
17.7	1.90(1)	0.78(1)	3.31(2)	8.0(1)	2.43(6)
20.4	1.91(1)	0.66(1)	3.29(2)	9.5(2)	2.87(8)
23.6	1.93(1)	0.64(1)	3.26(2)	9.8(2)	3.00(8)
26.5	1.93(1)	0.61(1)	3.25(2)	10.2(2)	3.15(9)
29.4	1.94(1)	0.57(1)	3.23(2)	11.1(3)	3.4(1)
34.5	1.95(1)	0.52(1)	3.22(2)	12.2(3)	3.8(1)
39.7	1.96(1)	0.47(1)	3.21(2)	13.4(4)	4.2(1)
44.1	1.97(1)	0.42(1)	3.19(2)	15.1(5)	4.7(2)
48.9	1.98(1)	0.39(1)	3.18(2)	16.1(6)	5.1(2)
55	2.00(1)	0.37(1)	3.15(2)	16.9(6)	5.4(2)
60	2.00(1)	0.35(1)	3.14(2)	18.0(7)	5.7(3)
65	2.00(1)	0.33(1)	3.14(2)	19.1(8)	6.1(3)
70	2.01(1)	0.33(1)	3.12(2)	19.3(8)	6.2(3)
75	2.03(1)	0.31(1)	3.10(2)	20.5(9)	6.6(3)
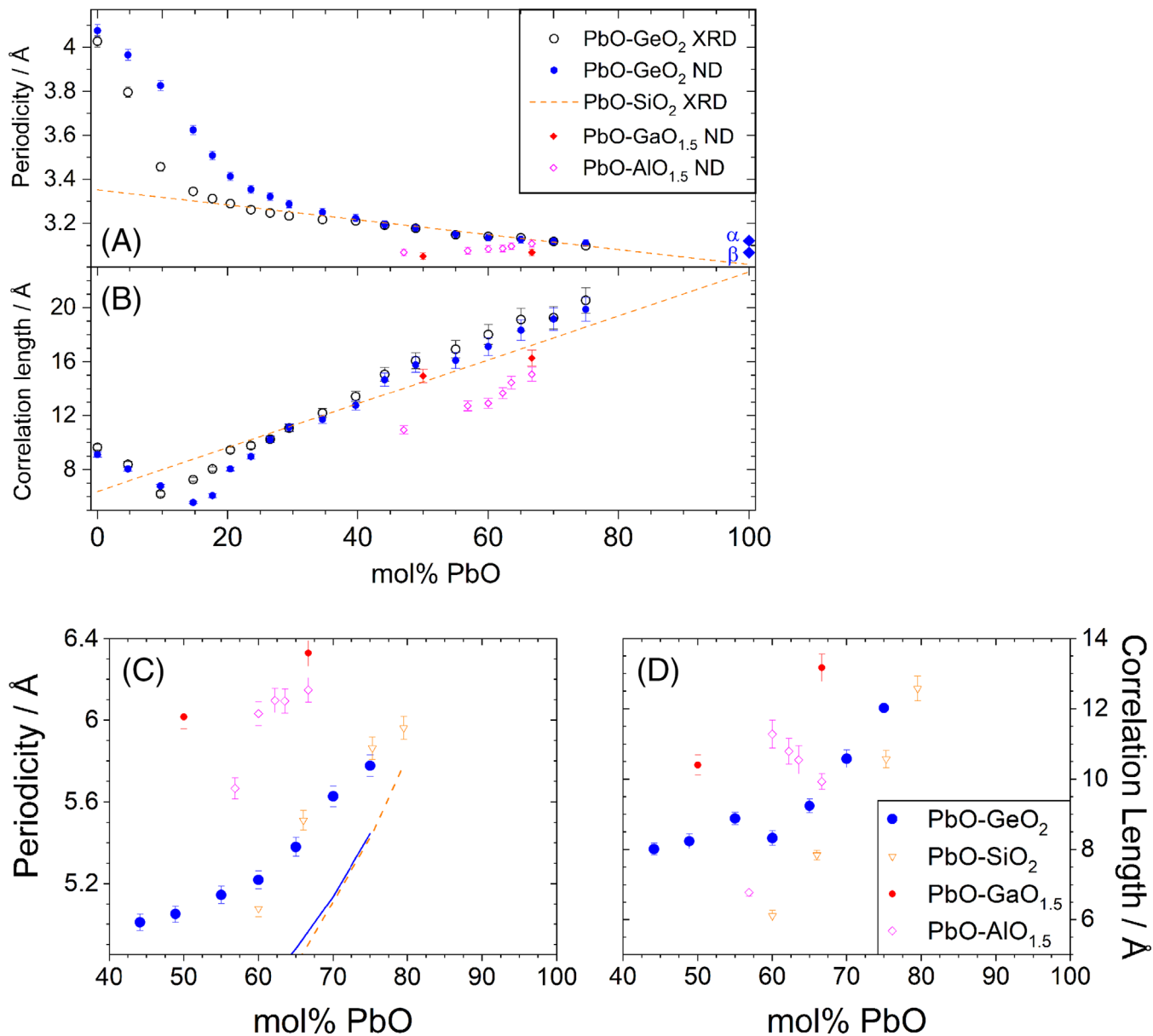
FIGURE 8 Periodicities and correlation lengths associated with (A,B) the FSDP in neutron and X-ray scattering and (C,D) the pre-peak in neutron scattering from lead germanate glasses. For comparison, the lines in (A,B) represent extrapolations of linear fits to the X-ray diffraction derived quantities for lead silicate glasses.[38,51] Data for lead aluminate[81] and gallate[82,83] glasses have also been included. The points in (A) marked α and β indicate the periodicities of the strongest X-ray Bragg peaks for crystalline α-PbO[84] and β-PbO.[85] Dashed and solid curves in (C) represent average Si–Si or Ge–Ge separations respectively, $r_{XX} = (c_X\rho_0)^{-1/3}$, $X =$ Si, Ge, based purely on the partial number densities $\rho_X = c_X\rho_0$

3.1.3 | Ge–O bond length distributions

Closer inspection of the Ge–O bond length distributions at ≈ 1.75 Å reveals that they exhibit asymmetry, particularly in the range $15 \lesssim x \lesssim 50$ mol% PbO, with a small broadening to the high r side. This is characteristic of the presence of Ge coordinated to greater than four oxygen ligands. Comparisons of three Ge–O bond length distributions with those of isomolar caesium[55] and calcium[53] germanate glasses containing approximately 79, 76, and 70 mol% GeO₂ are made

in Figure 11. This reveals that the asymmetry is less marked in the case of the lead germanate glasses. Table 4 summarizes the average Ge–O and O–Ge coordination numbers calculated by integration of $rT^N(r)$ from 1.52 Å up to the first minimum (beyond the peak maximum) which occurs at about 2.05 Å, approximately independent of the glass composition. n_{GeO} is plotted as a function of glass composition in Figure 1. As indicated by the small asymmetry of the Ge–O bond length distributions, the Ge–O coordination numbers are smaller in the PbO germanate system,

TABLE 4 Parameters derived from the Ge–O bond length distributions for lead germanate glasses. The fraction of $[GeO_5]$ units (assuming no $[GeO_6]$) is $N_5 = n_{GeO} - 4$. The fraction of $[GeO_6])$ units (assuming no $[GeO_5]$) is $N_6 = (n_{GeO} - 4)/2$. The fraction of NBOs is $f_{NBO} = 2 - n_{OGe}$, and the final column lists the number of NBOs per lead ion. Uncertainties in parentheses

Mol% PbO	r_{GeO} (Å)	n_{GeO}	N_5	N_6	n_{OGe}	f_{NBO}	NBO/Pb^{2+}
Plate quenched glasses							
0	1.7389(6)	3.98(1)	−0.02(1)	−0.01(1)	1.99(1)	0.012(2)	–
4.7(5)	1.740(3)	3.99(2)	−0.01(2)	0.00(1)	1.95(1)	0.053(3)	2.2(3)
9.7(5)	1.745(2)	3.95(2)	−0.05(2)	−0.03(1)	1.87(1)	0.127(2)	2.5(1)
14.7(5)	1.748(2)	4.14(2)	0.14(2)	0.07(1)	1.91(1)	0.094(2)	1.18(5)
17.7(5)	1.752(5)	4.06(2)	0.06(2)	0.03(1)	1.83(1)	0.167(4)	1.72(6)
20.4(5)	1.758(5)	4.11(2)	0.11(2)	0.06(1)	1.82(1)	0.178(4)	1.56(5)
23.6(5)	1.761(7)	4.06(2)	0.06(2)	0.03(1)	1.76(1)	0.243(5)	1.82(5)
26.5(5)	1.763(8)	4.14(3)	0.14(3)	0.07(1)	1.75(1)	0.246(7)	1.61(5)
29.4(5)	1.765(9)	4.11(3)	0.11(3)	0.06(1)	1.70(1)	0.299(7)	1.73(5)
34.5(5)	1.77(1)	4.07(3)	0.07(3)	0.03(2)	1.61(1)	0.390(8)	1.87(5)
39.7(5)	1.766(6)	4.06(3)	0.06(3)	0.03(1)	1.53(1)	0.473(4)	1.91(3)
44.1(5)	1.763(7)	3.98(3)	−0.02(3)	−0.01(2)	1.43(1)	0.572(4)	2.02(2)
48.9(5)	1.76(1)	3.99(4)	−0.01(4)	0.00(2)	1.35(1)	0.650(9)	2.01(3)
Twin-roller quenched glasses							
55.0(5)	1.758(2)	3.91(4)	−0.09(4)	−0.04(2)	1.21(1)	0.785(2)	2.07(2)
60.0(5)	1.761(3)	3.91(4)	−0.09(4)	−0.05(2)	1.12(1)	0.883(2)	2.06(1)
65.0(5)	1.760(1)	3.91(5)	−0.09(5)	−0.04(2)	1.01(1)	0.986(2)	2.05(1)
70.0(5)	1.76(1)	3.91(6)	−0.09(6)	−0.05(3)	0.90(1)	1.099(4)	2.04(1)
75.0(5)	1.76(1)	3.99(7)	−0.01(7)	−0.01(4)	0.80(1)	1.202(4)	2.00(1)

cf. the CaO and Cs$_2$O modified germanates. Furthermore, n_{GeO} is larger in the PbGe$_4$O$_9$[56,57] and PbGe$_3$O$_7$[58] crystal structures than in the glasses of similar composition. This is a qualitatively similar result to that found for the calcium germanate series.[53] In other words, whilst the n_{GeO} of the lead tetra- and trigermanate crystals (containing $[GeO_4]$ and $[GeO_6]$, and $[GeO_4]$ and $[GeO_5]$ respectively) follow the model predictions of Hannon et al.,[59] the lead germanate glasses either contain excess non-bridging oxygen (NBO) atoms, or else excess plumbite oxygen, that is oxygen bound to lead atoms alone, and not to any germanium. XPS[60] and ^{17}O NMR[61] measurements on the more widely studied lead silicate glasses would indicate that the concentration of plumbite oxygen in this composition region can be expected to be very low. Despite significant scatter of the $n_{GeO}(x)$ points, a broad maximum is apparent, with a peak value of $n_{GeO} = 4.14(3)$ at 26.5(5) mol% PbO, beyond which, at higher PbO contents, the coordination numbers decline toward the tetrahedral value of 4 at ≈ 50 mol% PbO. This result implies a maximum of 14(3)% of Ge atoms in five-fold coordination or 7(1)% in six-fold coordination. These are small fractions compared to the Ca and Cs modified germanate glasses, indicating that Pb is playing a different structural role.

Figure 12 compares the average Ge–O bond lengths, derived from the first moments of the Ge–O bond length distributions, of lead, calcium, and caesium germanate glasses. In the PbO–GeO$_2$ series, r_{GeO} increases upon addition of PbO, and passes through a maximum at 35 mol% PbO, similar to the behavior in CaO–GeO$_2$ glasses. The r_{GeO} in the lead germanate glasses are also systematically smaller than in the CaO–GeO$_2$ glasses, consistent with the smaller n_{GeO}. The position of the peak r_{GeO} at 35 mol% PbO, higher than the peak in n_{GeO}, indicates that there is another mechanism of bond elongation, in addition to the conversion of $[GeO_4]$ to $[GeO_5]$ or $[GeO_6]$. Indeed, this is supported by the fact that the average Ge–O bond length in PbO–GeO$_2$ glasses does not return to its value in pure GeO$_2$ glass (1.7382(6) Å) for $\gtrsim$ 50 mol% PbO, but appears to plateau at an intermediate value of ≈ 1.761 Å.

As for the Si–O bond length and Si–O–Si bond angle,[62,63] so r_{GeO} has been correlated with the reciprocal cosine of the Ge–O–Ge bond angle.[64] The Ge–O bond length is therefore also a function of the degree of s (or p) electron character of the oxygen, with greater s character correlating with shorter Ge–O bonds. Therefore, as in the lead silicates,[38,51] an increase in oxygen p character is expected with increasing PbO content owing to the increase of O–Pb coordination (Pb about a NBO) number and the reduction in Ge–O–Pb bond angle. In other words, the NBOs tend toward sp^3 hybridized $[OPb_3Ge]$ type environments, whilst
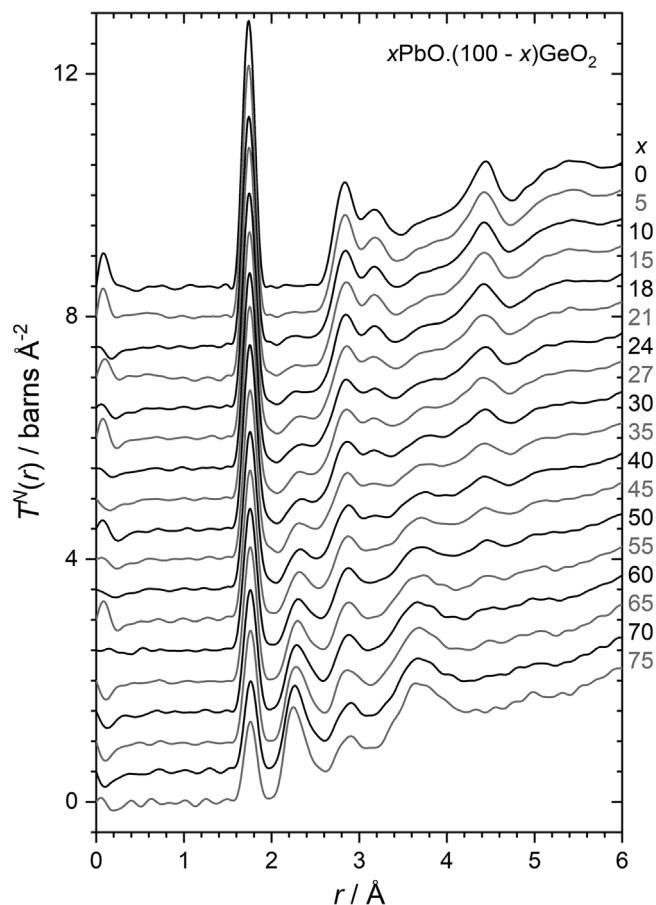
FIGURE 9 Neutron total correlation functions for lead germanate glasses. A Lorch[42] modification function and $Q_{max} = 40.00$ Å^{-1} were used. Molar compositions are indicated and vertical offsets have been used for clarity

FIGURE 10 X-ray total correlation functions for lead germanate glasses. A Lorch[42] modification function and $Q_{max} = 23.78$ Å^{-1} (plate-quenched glasses) and $Q_{max} = 23.62$ Å^{-1} (roller-quenched glasses) were used. Molar compositions are indicated and vertical offsets have been used for clarity. $T^X(r)$ for 75PbO.25SiO$_2$ glass[51] is shown for comparison (broken curve)

the contribution from Ge–O–Ge bonds decreases with the number of bridging oxygen atoms as the germanate network depolymerizes. These effects help to explain why the Ge–O bond length in the [GeO$_4$] tetrahedra is longer at high PbO content than in pure GeO$_2$ or at lower PbO content.

3.1.4 | Correlation function peak fits

In order to extract quantitative information on the Pb^{2+} environment, peak fitting to the total correlation functions was performed. The neutron $T^N(r)$ was fitted differently in the high PbO (> 50 mol%) and low PbO (≤ 50 mol%) regions. Low PbO compositions were fitted typically with two Ge–O peaks, as necessary to reproduce the asymmetric bond length distributions, along with the leading edges of the Pb–O peaks. Intrapolyhedral O–O correlations were not simulated due to the presence of multiple Ge centered polyhedral environments, with unknown geometries. Figure 13 shows an example fit for the $T^N(r)$
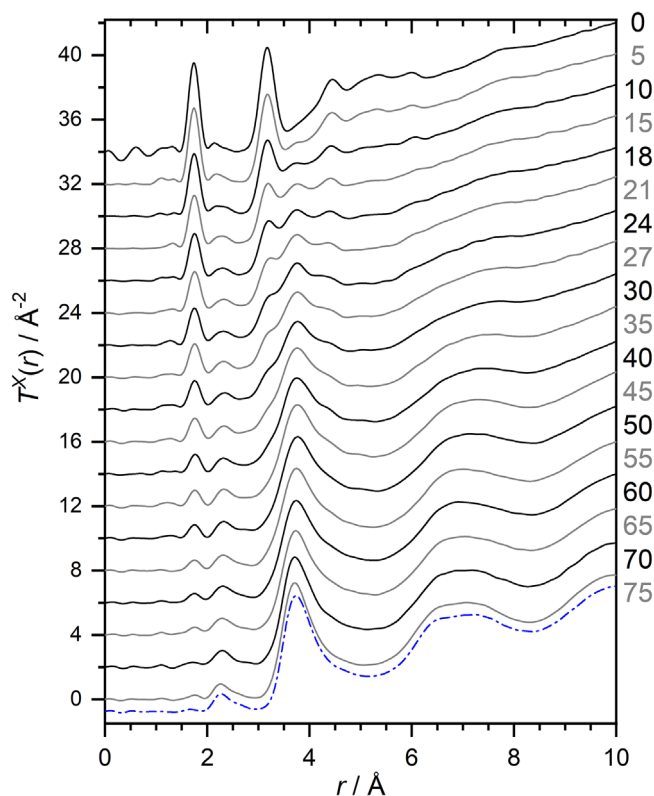
for 27PbO.73GeO$_2$ glass. Here, an O–O peak based on all Ge in ideal [GeO$_4$] tetrahedral sites has been simulated, with the width equal to that measured for vitreous germania. Owing to the total Ge–O coordination of 4.14(3), one would in fact expect a larger contribution to the correlation function from intrapolyhedral O–O pairs, and one which would be asymmetrically broadened to both the high r and low r sides of the O–O peak shown. This fact prevented the unambiguous fitting of Pb–O and/or O–O peaks to the ≈ 2.6 Å region.

For the high PbO composition glasses, a symmetric Ge–O peak in $T^N(r)$, coupled with lower n_{GeO}, close to four, was taken as evidence for all Ge in tetrahedral environments, and therefore the intrapolyhedral O–O peak could be more accurately simulated. Figure 13 shows an example fit for 75PbO.25GeO$_2$ glass in which the knowledge of the O–O contribution allows an additional Pb–O correlation to be fitted at 2.450(3) Å. Although additional intensity in the ≈ 2.6 Å region remains unassigned, at least part is likely due to Pb–O scattering pairs, as is evident from comparison to the X-ray diffraction derived $T^X(r)$.
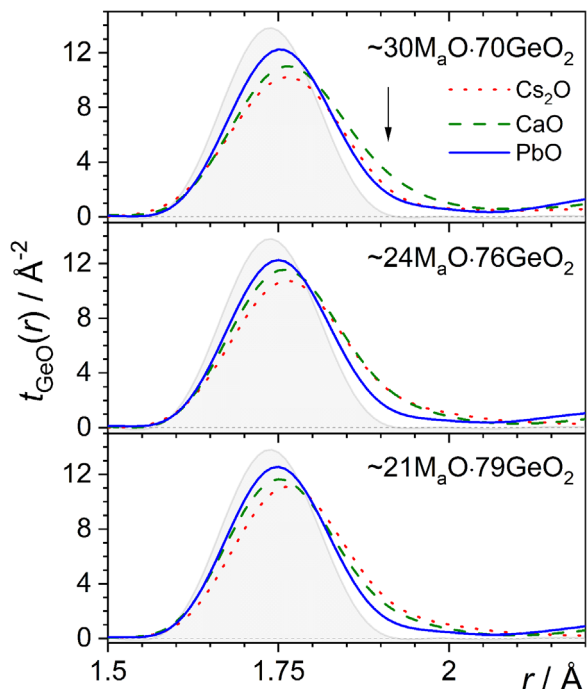
FIGURE 11 Ge–O bond length distributions (Equation (4)) from neutron diffraction on binary germanate glasses containing either caesium,[55] calcium[53] or lead, compared to that for pure GeO_2 glass (shaded). The arrow indicates the high r shoulder. A Lorch[42] modification function and $Q_{max} = 40$ Å^{-1} were used
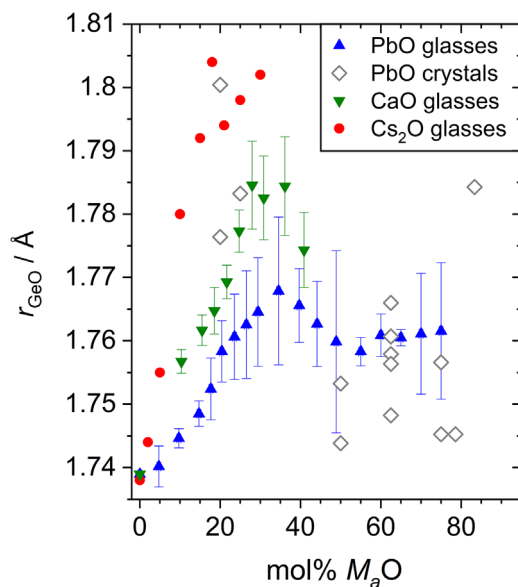

FIGURE 12 Average Ge–O bond lengths in lead germanate glasses, extracted by means of integration of $rT^N(r)$, as a function of glass composition. Values for ambient pressure crystalline lead germanates[30,56,57,67,74,75,28–92] as well as vitreous calcium[53] and caesium[55] germanates are shown for comparison. In colour online

The peaks fitted to the $T^N(r)$ measured by neutron diffraction have been weighted and broadened appropriately for comparison to $T^X(r)$ in Figure 13, for the 27 and 75 mol% PbO lead germanate glasses. In the former case, the residual at ≈ 2.6 Å is attributed to longer Pb–O bonds. In the case of the 75 mol% PbO germanate glass, the Pb–Pb peak has been estimated from that fitted to the leading edge of $T^X(r)$ for an 80PbO.20SiO$_2$ glass.[38] Given the small difference in PbO contents of the glasses, and the fact that small Pb–O and Pb–Si contributions were neglected in the fitting procedure, the Pb–Pb peak is likely an overestimate of the contribution to $T^X(r)$ for 75PbO.25GeO$_2$ glass. Therefore, the asymmetric contribution to the residual function between 3.0 and ≈ 3.6 Å (Figure 13) is likely underestimated in magnitude, and can be attributed predominantly to the Ge–Pb term, with some contribution from Pb–O (Ge–Ge, Ge–O, and O–O being small).

4 | DISCUSSION

4.1 | The germanate anomaly and the local structure about Ge^{4+}

Traditionally, as for the alkali and alkaline earth[53] germanate glasses, a maximum in mass density, as a function of glass composition, is taken as a defining characteristic of the germanate anomaly, but in the case of lead germanate glasses, this is not appropriate because the glass forming and modifying (or intermediate) oxides do not have similar masses. However, the atomic number density does show a clear maximum at ≈ 27 mol% PbO (Figure 2), which is only apparent as an inflection in the mass densities. This indicates that structural modifications of the glass are giving rise to a germanate anomaly in the PbO–GeO$_2$ system. What is more, an inflection is evident in the measured glass transition temperatures, again at ≈ 27 mol% PbO (Figure 3), which, similar to the mass density trend, may not appear as a clear maximum because of the dominant role of PbO, the addition of which decreases T_g. Note that Shelby[46] interpreted the plateau in $T_g(x)$ as due to phase separation, however, in the present DTA study, no higher temperature T_g was observed, likely due to the faster cooling rates applied during glass formation and the lack of subsequent annealing. We are therefore able to suggest that both the number density maximum, and the plateau observed in $T_g(x)$ are related to structural changes, and in particular, to the observed change in Ge–O coordination number (Figure 1).

Whilst very similar physical property trends have been measured before (see Figures 2 and 3), as well as maxima in resistivity,[25] and the Young's and shear moduli[26] at ~30 mol% PbO, the qualitatively similar trend in n_{GeO}

FIGURE 13 Example peak fits to neutron (upper) total correlation functions from (A) 27 and (B) 75 mol% PbO lead germanate glasses. A Lorch[42] modification function and $Q_{max} = 40.00$ Å^{-1} were used. Pb–O peaks have been fitted at ~2.25 Å. Two peaks have been used to reproduce the asymmetric Ge–O bond length distribution in 27PbO.73GeO$_2$. Intratetrahedral O–O correlations have been calculated in both cases based on all Ge in ideal [GeO$_4$] tetrahedral sites. This is a valid model in 75PbO.25GeO$_2$, allowing a second Pb–O correlation to be fitted at ~2.45 Å, but in 27PbO.73GeO$_2$, the intrapolyhedral O–O correlation would likely be broadened asymmetrically to both sides due to the presence of [GeO$_5$] and/or [GeO$_6$]. The fits to the neutron $T^N(r)$ are compared to the X-ray $T^X(r)$ in the lower panels (C) and (D), where the Pb–Pb correlation estimated for 80PbO.20SiO$_2$ glass[38,51] is also compared to $T^X(r)$ for 75PbO.25GeO$_2$ (green curve). In color online
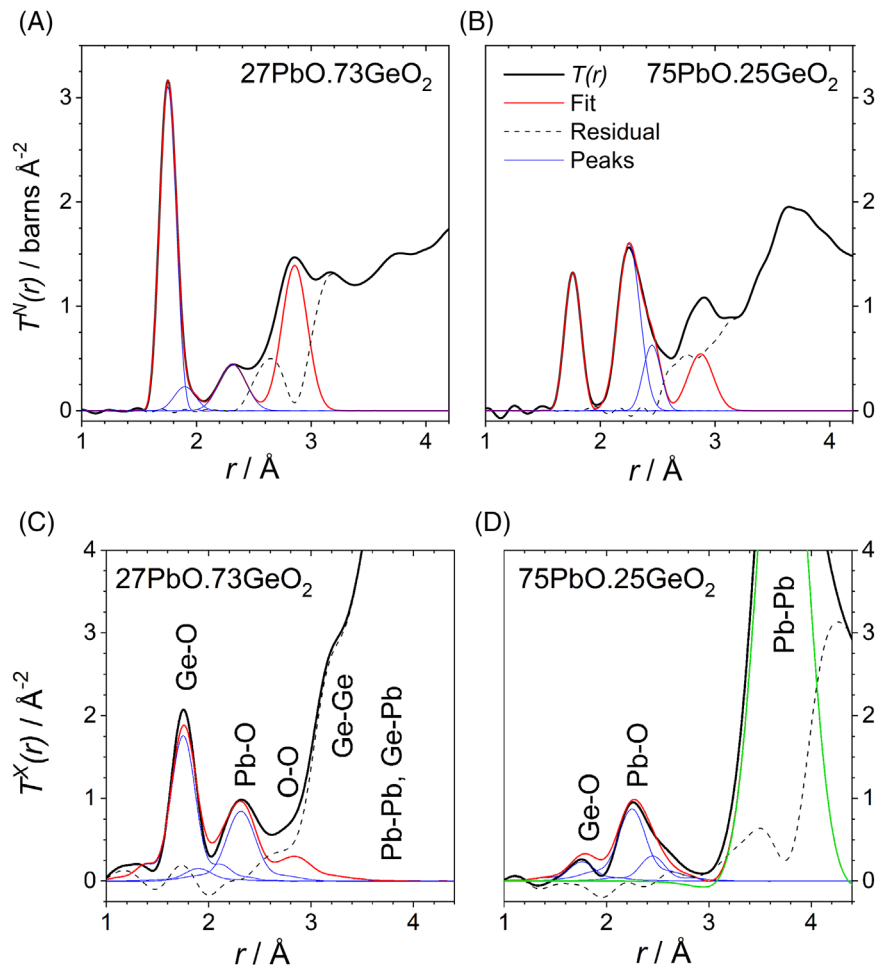
has not previously been measured, see Figure 1A. We have previously shown[20] that the coordination numbers published in an earlier neutron diffraction study[21] were erroneously high, whilst EXAFS measurements[11,13,14,15] are known to have larger uncertainties compared to high-resolution diffraction (where directly comparable) owing to the limited Q range accessible which leads to strongly correlated n_{jk} and thermal width/disorder parameters. It is interesting to note that one Ge K-edge EXAFS study[15] does report a maximum in n_{GeO}, although it is larger, and at lower PbO content, than in the present study. Remarkably, a classical molecular dynamics study[17] reports the closest agreement to the present results, despite the arguably inappropriate use of isotropic (non-polarizable) potentials for a LP cation such as Pb^{2+}. The present measurements of $n_{GeO}(x)$ appear to be the most consistent with the measured "anomalous" physical properties of lead germanate glasses, especially in terms of the position of the broad maximum in $n_{GeO}(x)$. Meanwhile, the depressed magnitude of the $n_{GeO}(x)$ maximum, compared to alkali and alkaline earth germanate glasses, is consistent with the measured structural role of Pb^{2+}, as discussed below.

Although it is not possible to state the nature of the more highly coordinated germanate species, be they five-fold GeO$_5$ or six-fold GeO$_6$, we can say that at least for the 40 mol% PbO glass, there are likely to be GeO$_6$ octahedra present. This follows the same argument as that applied to calcium germanate glasses,[53] where Ge–O coordination numbers between the model[59] curves for GeO$_5$ and GeO$_6$ (Figure 1) imply that GeO$_6$ must be present, or else assumptions of the models do not hold. These assumptions include that there are no bridges between GeO$_n$ ($n = 5$, 6) units, so an alternative possibility is that there is a small amount of such bridges in the 40PbO.60GeO$_2$ glass. Importantly, none of the measured n_{GeO} exceed the model curve for GeO$_6$ as the $n > 4$ species, and this implies that the charge avoidance aspect of the models holds overall, whether or not there is a local breaking of this assumption through the presence of bridges between GeO$_n$ ($n = 5$, 6). That said, asymmetry in the Ge–O peak is observed up to 50 mol% PbO, implying the presence of small amounts of GeO$_n$ ($n = 5$, 6) even up to this composition, which would require further violation of the charge avoidance-based models.

4.2 | Molar volumes and atom number densities

Before discussing the structural role of Pb^{2+} in the lead germanate glasses, it is worth comparing their atom number densities and molar volumes to those of the alkaline earth germanates, as in Figure 2. While the lead germanate glass number densities do show a maximum characteristic of a germanate anomaly, it is clearly less pronounced than in the alkaline earth germanate glasses. Furthermore, at low MO content, the PbO germanate glasses do not follow the constant volume per mole $JMO.GeO_2$ predictions, as the alkaline earth germanates do. This indicates that Pb^{2+} does not simply occupy the voids within the germanate network in this composition range, but plays a different structural role, occupying more volume - akin to a network modifier, which we relate to the suppressed values of $n_{GeO}(x)$ compared to the $CaO–GeO_2$ (and presumably other alkaline earth germanate) glasses.

Put another way, if Pb^{2+} were to behave like a typical alkaline earth network modifier, we would expect the atom number densities and molar volumes to be similar to those for $SrO–GeO_2$ glasses, based on the similar ionic radii of Pb^{2+} and Sr^{2+} (Figure 2C).[65] Since this is not the case, we infer a different structural role for Pb^{2+}, as evidenced by our structural measurements.

4.3 | The structural role of Pb^{2+}

The presence of short Pb–O bonds (≈ 2.3 Å) in all glasses implies the presence of at least a fraction of Pb^{2+}, in all cases, with a low coordination number to oxygen. This in itself implies an asymmetric distribution of more strongly bound ligands due to the presence of a stereochemically active lone pair of electrons, and Pb^{2+} thereby plays a role with some glass-network-forming character, as opposed to a purely modifying one. This is supported by the 207-Pb NMR spectra, Figure 4, which have mean chemical shifts, δ_{iso}, in the range -70 ± 50 ppm (27 mol% PbO) to $+980 \pm 50$ ppm (75 mol % PbO). These are within the known range[33] for covalently bonded compounds, as opposed to more ionically (more highly coordinated) bonded lead, with more negative δ_{iso}. At high PbO content, as in the silicate glasses, the 207-Pb NMR lineshape approaches that for an axially symmetric chemical shift tensor, characteristic of the pyramidal sites found in crystalline PbO polymorphs.

Figure 14 displays the parameters obtained from fitting to the leading edge of the Pb–O peak (at ≈ 2.3 Å) in the neutron $T^N(r)$ (Figure 13). Note that, by analogy to the silicate glasses,[38,51] additional, longer Pb–O bonds (≈ 2.5 Å) are expected in all cases, and this is indeed evident in Figure 13

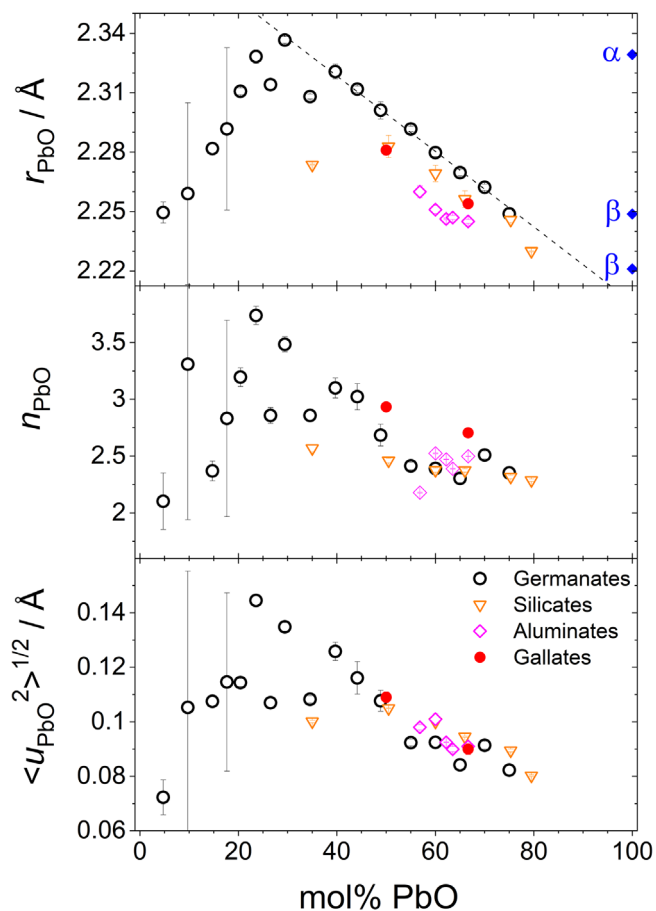**FIGURE 14** Parameters characterizing the distribution of short Pb–O bonds in binary lead germanate, silicate,[38,51] aluminate[81] and gallate[82,83] glasses (the latter compositions are defined $PbO–(Al,Ga)O_{1.5}$, as in Figures 8 and 9). The points marked α and β indicate Pb–O bond lengths in crystalline α-PbO[84] and β-PbO.[85] The average *short* Pb–O bond lengths, coordination numbers and RMS bond length variations were obtained from peak fitting to the leading-edge of the Pb–O peak in neutron total correlation functions (Figure 13)

for the high PbO content glass $T^N(r)$, and the X-ray $T^X(r)$, at both high and low PbO content. Nonetheless, the trends revealed in Figure 14 provide some important insights. Despite evidence of correlations between the fit parameters, the following statements can be made. The most accurately determined parameters are the r_{PbO} (Figure 14) which pass through a maximum at approximately the same glass composition as do the average r_{GeO} (Figure 12) and the n_{GeO} (Figure 1). The Pb–O and Ge–O parameters are related as a result of bonds from Pb^{2+} to bridging oxygen (Ge–O–Ge) which are under bonded by germanium alone as a result of the presence of five- or six-fold Ge centered polyhedra. This implies the presence of some Pb^{2+} playing a more network modifying role *cf.* $PbO–SiO_2$ glasses.[38,51]

The Pb–O coordination numbers and RMS bond length deviations, Figure 14, are less well determined than the

bond lengths themselves because they are more prone to uncertainties arising from baseline oscillations (reciprocal space noise), overlap with other contributions to $T^N(r)$, and normalization (and glass composition and density) in the case of the n_{PbO}. Nonetheless, the Pb–O coordination numbers do indeed tend to follow the trend of the r_{PbO}, passing through a maximum, despite considerable scatter, which correlates with the scatter in the measured peak widths, $\langle u_{PbO}^2 \rangle^{1/2}$, and positions, r_{PbO}.

By direct comparison to the results from lead silicate glasses,[38,51] Figure 14, it is clear, particularly at $\approx$ 35 mol% PbO, that both r_{PbO} and n_{PbO} are larger in the germanate glass, than in the silicate. At higher PbO contents the n_{PbO} converge, whilst the r_{PbO} remain marginally ($\approx$ 1 pm) longer in the germanates, which can be attributed to the higher electronegativity of Ge compared to Si.[66]

Therefore Pb^{2+} has, on average, more network modifier character at compositions where $[GeO_5]$ and/or $[GeO_6]$ are present. A similar effect is present, to a much greater extent, in crystalline lead germanates, where, for example, Pb may be isomorphous with Ba or Sr (α-PbGe$_4$O$_9$[57]), playing a pure network modifying role, or may occupy distorted seven-fold sites (γ-PbGe$_4$O$_9$[56] and PbGe$_3$O$_7$[67]), playing an intermediate role. However, it is important to remember that the n_{GeO} and the r_{GeO} measured for the crystals are significantly larger than those for the glasses (Figures 1 and 12), and that the differences in Pb environment for high and low PbO content germanate glasses are therefore more subtle. This can be contrasted to lead borate glasses, where both diffraction[68,69] and 207-Pb NMR[70,71,72] clearly show a change of Pb–O coordination from high (modifier-like) at low PbO contents, to low (former-like) at high PbO contents. The fact that this is concomitant with a strong change in boron–oxygen coordination number (and borate anomaly) is consistent with our arguments linking the subtle changes in Pb–O environment in lead germanate glasses to the weak change in germanium–oxygen coordination number and consequent weak germanate anomaly.

The total neutron scattering measurements do not distinguish between all Pb on intermediate (γ-PbGe$_4$O$_9$[56] and PbGe$_3$O$_7$[67]) type sites, or a mixture of network forming plus modifying and/or intermediate type sites. However, what is clear from the magnitude of the n_{PbO} in Figure 14 (close to 3 to 4 as expected from the r_{PbO} and bond-valence considerations), is that any network modifying Pb must be in the minority, and it is not necessary to invoke a bimodal network former + modifier picture when the crystal chemistry so clearly demonstrates the flexibility of the Pb^{2+} bonding and oxygen coordination shell, such that single sites can be considered themselves as intermediate (with respect to glass network formation).

4.4 | Intermediate-range order

There are at least three separate features evident in the low-Q X-ray and neutron scattering functions which yield insight into the intermediate range ordering in the lead germanate glasses.

Firstly, the first sharp diffraction peaks. At low PbO contents, the FSDPs are characterized by large periodicities and short correlation lengths (Figure 8A,B), characteristic of the germanate network and typically attributed to the correlations between rings in the relatively open germanate framework. As PbO is added there is a transition toward shorter periodicities and longer correlation lengths as Pb-X pair terms begin to dominate the scattering. These features are characteristic of the plumbite glass network,[38] and are dominated by Pb–Pb, and in the present case possibly also Pb–Ge, correlations. The approach of the periodicity to that present in the PbO polymorphs, combined with the correlation length exceeding 2 nm, almost 4 to 5 times the mean unit cell parameter of β-PbO or α-PbO respectively, can be expected to have strong implications for the glass forming limit in this system. That said, it is not expected that these phases crystallize out during devitrification, or during quenching at subcritical rates, but rather the mixed lead germanate phases indicated in Figure 12. It is noteworthy that the FSDP correlation lengths exceed those observed in isomolar lead silicate glasses, indicating a more well-developed plumbite network intermediate-range ordering, which could well relate to the somewhat greater tendency toward crystallization in the germanate melts.

Secondly, the pre-peaks that are most clearly apparent in the neutron structure factors for high PbO glasses indicate ordering on longer length scales than the FSDP. These have similar periodicities and correlation lengths to the features observed for lead silicate glasses (Figure 8C,D), and so by analogy can be attributed to correlations between isolated germanate polyanions such as GeO$_4^{4-}$ (Q^0) monomers, Ge$_2$O$_7^{6-}$ (Q^1) dimers, and at lower PbO contents, likely short chains and/or rings involving Q^2 units. The fact that the periodicities are larger than the mean Ge–Ge separation, based on the Ge partial number density (Figure 8C), indicates that there is indeed some degree of polymerization retained between germanate units, right up to the highest PbO contents. This is similar to observations in lead silicate glasses. As for the FSDPs, the pre-peaks are characterized by longer correlation lengths in the germanate glasses compared to the silicates, again indicating a better developed medium-range ordering. However, it should be noted that the germanate units are larger than silicate units, likely contributing to the slightly lower atom number densities in the germanate glasses (Figure 2A). Indeed the Ge–O bond is about 8% longer than the

Si–O bond, which can be compared to correlation lengths between 50% and 13% longer in the 60 to 75 mol% PbO range respectively.

Thirdly, the SAXS observed at our lowest experimental Q values, Figure 7, indicate that as PbO is introduced into the germanate network it does not enter homogeneously. This is supported by the SAXS intensity corresponding to length scales $2\pi/Q_{SAXS} > r_{PbPb} = (c_{Pb}\rho_0)^{-1/3}$, that is, exceeding the mean Pb–Pb separation based on the partial number density of Pb. At its highest, this latter value is close to 1 nm in the 5 mol% PbO glass, whilst $2\pi/Q_{SAXS} > 2\pi/Q_{min} = 1.4$ nm. At 24 mol% PbO, a weak maximum in the SAXS becomes apparent, with $2\pi/Q_{SAXS} \approx 8.5$ Å, which compares to a calculated $r_{PbPb} = 5.6$ Å. Thus some clustering of Pb atoms in the glasses with < 50 mol% PbO is apparent, something which also occurs in the lead silicate glasses, and likely arises as a result of sharing of NBO by more than one Pb cation. Based on earlier studies,[25,46] this clustering is likely a pre-cursor to phase-separation occurring on longer length scales after heat treatment, or slower initial cooling of the glasses, and corresponds to the early stages of spinodal decomposition.[49] Our results apply to the rapidly quenched glasses of the present study, and the interplay between short-range structure, thermal history and longer range structures arising from inhomogeneity and phase separation remains a topic for future investigations.

5 | CONCLUSION

Lead germanate glasses exhibit a wonderful interplay between the local structures of the two cationic species, Pb^{2+} and Ge^{4+}, resulting in behavior qualitatively intermediate between that observed in lead silicate and lead borate glasses.

Overall, structural behavior is similar to that in lead silicate glasses, with most germanium tetrahedrally four-fold coordinated to oxygen, and divalent lead acting largely like a network former, having low coordination number to oxygen and a stereochemically active lone electron pair. However, at low PbO contents from $5 \leq$ mol% PbO ≤ 40, experimental evidence strongly supports the existence of a fraction of germanium with 5 or 6 oxygen neighbors—a key factor in causing "germanate anomaly" extrema observed in the physical properties of lead germanate glasses. These more highly coordinated germanate species, GeO_5 or GeO_6, indicate some network modifier character in the role played by Pb^{2+}. Indeed, one would expect more ionic, longer and weaker Pb–O bonds to form to the bridging oxygen atoms linked to GeO_5 or GeO_6 units, which are overall under-bonded by germanium alone. This is borne out experimentally in the elongation observed, of even the short Pb–O bonds, correlating with the amount of GeO_5

or GeO_6 present—direct evidence for a partial modifier character for Pb^{2+} in this composition region.

The modifier character of Pb^{2+} is nonetheless weaker than that observed for alkaline earths in germanate glasses, as evidenced by the smaller factions of GeO_5 or GeO_6. Thus we refer to the "weak germanate anomaly" in lead germanate glasses, which is also evident when comparing the molar volumes of lead and alkaline earth germanate glasses. The germanate anomaly in lead germanate glasses is also "weak" with respect to the "borate anomaly" in lead borate glasses. In the lead borate glasses, there is a strong change in boron–oxygen coordination number with composition, similar to alkali and alkaline earth borate glasses, which correlates with a much more drastic change in the local environment of lead, from modifier-like at low PbO contents, to network former-like at high PbO contents.

These conclusions correspond to the rapidly quenched glasses studied which exhibit nanoscale heterogeneity at low PbO contents, as evidenced by small-angle X-ray scattering, and consistent with the early stages of spinodal decomposition. Low PbO content germanate glasses cooled more slowly, or annealed, could coarsen and show phase separation on longer length scales, which may affect the average short-range structures observed, although we have demonstrated previously by neutron diffraction that such effects are small at 40 mol% PbO.[20]

ORCID

Oliver L. G. Alderman https://orcid.org/0000-0002-2342-811X
Alex C. Hannon https://orcid.org/0000-0001-5914-1295

REFERENCES

1. Munasinghe HT, Winterstein-Beckmann A, Schiele C, Manzani D, Wondraczek L, Afshar S, et al. Lead-germanate glasses and fibers: a practical alternative to tellurite for nonlinear fiber applications. Opt Mater Express. 2013;3(9):1488–503.
2. Cereyon A, Champagnon B, Martinez V, Maksimov LV, Yanush OV, Bogdanov VN. xPbO–(1 – x)GeO₂ glasses as potential materials for Raman amplification. Optical Mater. 2006;28:1301–4.
3. Żur L. Structural and luminescence properties of Eu³⁺, Dy³⁺ and Tb³⁺ ions in lead germanate glasses obtained by conventional high-temperature melt-quenching technique. J Mol Str. 2013;1041:50–4.

4. Lezal D, Pedlikova J, Horak J. GeO$_2$-PbO glassy system for infrared fibers for delivery of Er:YAG laser energy. J Non-Cryst Solids. 1996;196:178–82.

5. Wang J, Lincoln JR, Brocklesby WS, Deol RS, Mackechnie CJ, Pearson A, et al. Fabrication and optical-properties of lead-germanate glasses and a new class of optical fibers doped with Tm^{3+}. J Appl Phys. 1993;73(12):8066–75.

6. Lincoln JR, Brocklesby WS, Mackechnie CJ, Wang J, Deol RS, Hanna DC, et al. New class of fiber laser based on lead-germanate glass. Electron Lett. 1992;28(11):1021–2.

7. Dussauze M, Giannoudakos A, Velli L, Varsamis CPE, Kompitsas M, Kamitsos EI. Structure and optical properties of amorphous lead-germanate films developed by pulsed-laser deposition. J Chem Phys. 2007;127(3) 034704.

8. Nasu H, Ito Y, Yamamoto Y, Hashimoto T, Kamiya K. Second-harmonic generation from thermally poled PbO-GeO$_2$ glasses. J Ceram Soc Jpn. 2001;109(4):366–8.

9. Margaryan AA. Germanium dioxide-based glasses as advanced optical sensors materials. In: Nalwa HS, editor. Photodetectors and fiber optics. Academic Press; 2001. p. 369–458.

10. Sigaev VN, Gregora I, Pernice P, Champagnon B, Smelyanskaya EN, Aronne A, et al. Structure of lead germanate glasses by Raman spectroscopy. J Non-Cryst Solids. 2001;279(2-3):136–44.

11. Ribeiro SJL, Dexpertghys J, Piriou B, Mastelaro VR. Structural studies in lead germanate glasses - EXAFS and vibrational spectroscopy. J Non-Cryst Solids. 1993;159(3):213–21.

12. Canale JE, Condrate RA, Nassau K, Cornilsen BC. Characterization of various glasses in the binary PbO-GeO$_2$ and Bi$_2$O$_3$-GeO$_2$ systems. J Can Ceram Soc. 1986;55:50–6.

13. Ghigna P, Mustarelli P, Tomasi C, Quartarone E, Scavini M, Speghini A, et al. A combined nuclear magnetic resonance and X-ray absorption fine structure study on the local structures of Ge and Pb in PbO-GeO$_2$ glasses and their relationships with thermal properties and devitrification products. J Phys Chem B. 2002;106(38):9802–9.

14. Witkowska A, Sikora B, Trzebiatowski K, Rybicki J. Germanate anomaly in heavy metal oxide glasses: an EXAFS analysis. J Non-Cryst Solids. 2006;352(40-41):4356–61.

15. Yamamoto H, Kamiya K, Matsuoka J, Nasu H. EXAFS study on the coordination state of germanium in PbO-GeO$_2$ glasses - relation between structure and optical nonlinearity. J Ceram Soc Jpn. 1993;101(9):974–9.

16. Witkowska A, Madecka A, Trzebiatowski K, Dziedzic J, Rybicki J. EXAFS analysis of local neighbourhood of Pb atoms in lead-germanate glasses. Rev Adv Mater Sci. 2006;12(2):112–9.

17. Ghobadi E. Molecular dynamics simulation of lead germanate glasses. PhD thesis, The Department of Chemistry and Biochemistry, Concordia University, Montreal, 2008, p. 148.

18. Rybicki J, Witkowska A, Bergmanski G, Bosko J, Mancini G, Feliziani S. The Structure of Rarefied and Densified PbGeO$_3$ and PbGeO$_2$ Glasses: A Molecular Dynamics Study. Comput Methods Sci Technol. 2001;7(1):91–112.

19. Nanba T, Miyaji T, Takada J, Osaka A, Miura Y, Yasui I. Computer-simulation on the structure and vibrational-spectra in Ge-Pb-O-F glass. J Non-Cryst Solids. 1994;177:131–6.

20. Alderman OLG, Hannon AC, Holland D, Umesaki N. On the germanium-oxygen coordination number in lead germanate glasses. J Non-Cryst Solids. 2014;386:56–60.

21. Umesaki N, Brunier TM, Wright AC, Hannon AC, Sinclair RN. Neutron-scattering from PbO-GeO$_2$ glasses. Phys B. 1995;213:490–2.

22. Bogdanov VN, Anan'ev AV, Golubkov VV, Golovnev AV, Maksimov LV, Pakhnin AY, et al. Micro- and nanoinhomogenities in glasses and their melts studied by optical, SAXS, acoustical and thermodynamic methods. J Phys Conf Ser. 2007;93:012033.

23. Cervinka L, Bergerova J, Sigaev VN, Rocca F. Structure of (GeO$_2$)(1-x)(PbO)(x) glasses by X-ray scattering. J Non-Cryst Solids. 2001;293:502–9.

24. Nouri M, Alizadeh P, Tavoosi M. The relationship between structural and optical properties of GeO$_2$-PbO glasses. J Adv Mater Process. 2017;5(2):3–10.

25. Topping JA, Harrower IT, Murthy MK. Properties and structure of glasses in system PbO-GeO$_2$. J Am Ceram Soc. 1974;57(5):209–12.

26. Topping JA. Elastic properties of glasses in system PbO-GeO$_2$. J Am Ceram Soc. 1974;57(10):455.

27. Revised Nuffield Advanced Science Book of Data. Longman, (1985).

28. Iwata Y, Koyano N, Shibuya I. Neutron-diffraction studies of ferroelectric 5PbO.3GeO$_2$ above curie-point. J Phys Soc Jpn. 1973;35(4):1269.

29. Iwata Y, Koizumi H, Koyano N, Shibuya I, Niizeki N. Crystal-structure determination of ferroelectric phase of 5PbO.3GeO$_2$. J Phys Soc Jpn. 1973;35(1):314.

30. Ivanov SA, Rannev NV, Bush AA, Leichenko AI, Venevtsev YN. Investigation of the crystal-structure of high-temperature phase Pb$_3$GeO$_5$. Kristallografiya. 1979;24(2):252–6.

31. Havel AJ, Feller SA, Affatigato M, Karns M, Karns M. Design and operation of a new roller quencher for rapidly cooling melts into glasses. Glass Technol.: Eur J Glass Sci Technol A. 2009;50(4):227–9.

32. Holland D, Feller SA, Kemp TF, Smith ME, Howes AP, Winslow D, et al. Boron-10 NMR: what extra information can it give about borate glasses? Phys Chem Glasses-B. 2007;48(1):1–8.

33. Fayon F, Farnan I, Bessada C, Coutures J, Massiot D, Coutures JP. Empirical correlations between Pb-207 NMR chemical shifts and structure in solids. J Am Chem Soc. 1997;119(29):6837–43.

34. Hannon AC. Results on disordered materials from the General materials diffractometer, GEM, at ISIS. Nucl Instrum Meth A. 2005;551(1):88–107.

35. Poulsen HF, Neuefeind J, Neumann HB, Schneider JR, Zeidler MD. Amorphous silica studied by high-energy X-ray-diffraction. J Non-Cryst Solids. 1995;188(1-2):63–74.

36. Bouchard R, Hupfeld D, Lippmann T, Neuefeind J, Neumann HB, Poulsen HF, et al. A triple-crystal diffractometer for high-energy synchrotron radiation at the HASYLAB high-field wiggler beamline BW5. J Synchrotron Radiat. 1998;5:90–101.

37. Bearden JA, Burr AF. Reevaluation of X-Ray Atomic Energy Levels. Rev Mod Phys. 1967;39(1) 125–42.

38. Alderman OLG, Hannon AC, Holland D, Feller S, Lehr G, Vitale AJ, et al. Lone-pair distribution and plumbite network formation in high lead silicate glass, 80PbO.20SiO$_2$. Phys Chem Chem Phys. 2013;15(22):8506–19.

39. Hannon AC, Howells WS, Soper AK. Atlas - a suite of programs for the analysis of time-of-flight neutron-diffraction data from liquid and amorphous samples. Inst Phys Conf Ser. 1990;(107):193–211.

40. Finbak C. The structure of liquids .1. Acta Chemica Scandinavica. 1949;3(10):1279–92.

41. Waasmaier D, Kirfel A. New analytical scattering-factor functions for free atoms and ions. Acta Crystallogr A. 1995;51:416–31.

42. Lorch E. Neutron diffraction by germania, silica and radiation-damaged silica glasses. J Phys C Solid State Phys. 1969;2:229.

43. Sears VF. Neutron scattering lengths and cross sections. Neutron News. 1992;3(3):26–37.

44. Faber T, Ziman J. A theory of the electrical properties of liquid metals. Philos Mag. 1965;11(109):153–73.

45. Keen DA. A comparison of various commonly used correlation functions for describing total scattering. J Appl Crystallogr. 2001;34:172–7.

46. Shelby JE. Properties and structures of RO-GeO$_2$ glasses. J Am Ceram Soc. 1983;66(6):414–6.

47. SciGlass Professional 7.3. ITC Inc., (2008).

48. Di Martino D, Santos L, Almeida R. Germanate anomaly in sodium and caesium binary glass systems: a comparison. Phys Chem Glasses. 2004;43C:85–9.

49. Morinaga K, Nakashima K. Phase-separation in germanate glasses. J Non-Cryst Solids. 1988;103(1):108–16.

50. Feller S, Lodden G, Riley A, Edwards T, Croskrey J, Schue A, et al. A multispectroscopic structural study of lead silicate glasses over an extended range of compositions. J Non-Cryst Solids. 2010;356(6-8):304–13.

51. Alderman OLG, Hannon AC, Holland D, Dupree R, Feller S, Lehr G, et al. Lead silicate glass structure: new insights from diffraction and modelling of probable lone pair locations. J Am Ceram Soc. 2021, https://doi.org/10.1111/jace.18125

52. Massiot D, Fayon F, Capron M, King I, Le Calve S, Alonso B, et al. Modelling one- and two-dimensional solid-state NMR spectra. Magn Reson Chem. 2002;40(1):70–6.

53. Alderman OLG, Hannon AC, Feller S, Beanland R, Holland D. The germanate anomaly in alkaline earth germanate glasses. J Phys Chem C. 2017;121(17):9462–79.

54. Hussin R, Dupree R, Holland D. The Ge-O-Ge bond angle distribution in GeO$_2$ glass: a NMR determination. J Non-Cryst Solids. 1999;246(3):159–68.

55. Hannon AC, Di Martino D, Santos LF, Almeida RM. Ge-O coordination in cesium germanate glasses. J Phys Chem B. 2007;111(13):3342–54.

56. Shashkov AY, Rannev NV, Venevtsev YN. The crystalline-structure of lead gamma-tetragermanate. Zh Neorg Khim+. 1981;26(11):2926–8.

57. Shashkov AY, Efremov VA, Matsichek I, Rannev NV, Venevtsev YN, Trunov VK. Crystalline-structure of lead alpha-tetragermanate alpha-PbGe$_4$O$_9$. Zh Neorg Khim+. 1981;26(3):583–7.

58. Otto HH. Crystal-structure of PbGe$_3$O$_7$ with Ge(4+) in trigonal-dipyramidal along with tetrahedral coordination. Z Kristallogr. 1979;149(3-4):197–205.

59. Hannon AC, Di Martino D, Santos LF, Almeida RM. A model for the Ge-O coordination in germanate glasses. J Non Cryst Solids. 2007;353(18-21):1688–94.

60. Nesbitt HW, Bancroft GM, Henderson GS, Sawyer R, Secco RA. Direct and indirect evidence for free oxygen (O^{2-}) in MO-silicate glasses and melts (M = Mg, Ca, Pb). Am. Miner. 2015;100(11-12):2566–78.

61. Lee SK, Kim EJ. Probing metal-bridging oxygen and configurational disorder in amorphous lead silicates: insights from ^{17}O solid-state nuclear magnetic Resonance. J Phys Chem C. 2015;119(1):748–56.

62. Gibbs GV, Hill FC, Boisen MB. The SiO bond and electron density distributions. Phys Chem Miner. 1997;24(3):167–78.

63. Boisen MB, Gibbs GV, Downs RT, Darco P. The dependence of the sio bond length on structural parameters in coesite, the silica polymorphs, and the clathrasils. Am Miner. 1990;75(7-8):748–54.

64. Hill RJ, Louisnathan SJ, Gibbs GV. Tetrahedral bond length and angle variations in germanates. Aust J Chem. 1977;30(8):1673–84.

65. Dronskowski R. Computational chemistry of solid state materials, Vol. 300, Weinheim: Wiley; 2005.

66. Gibbs GV, Boisen MB, Hill FC, Tamada O, Downs RT. SiO and GeO bonded interactions as inferred from the bond critical point properties of electron density distributions. Phys Chem Miner. 1998;25(8):574–84.

67. Otto HH. Crystal-structure of PbGe$_3$O$_7$ with Ge(4+) in trigonal-dipyramidal along with tetrahedral coordination. Z Kristallogr. 1979;149(3-4):197–205.

68. Ushida H, Iwadate Y, Hattori T, Nishiyama S, Fukushima K, Ikeda Y, et al. Network structure of B$_2$O$_3$-PbO and B$_2$O$_3$-PbO-PbBr$_2$ glasses analyzed by pulsed neutron diffraction and Raman spectroscopy. J Alloy Compd. 2004;377(1–2):167–73.

69. Takaishi T, Jin JS, Uchino T, Yoko T. Structural study of PbO-B$_2$O$_3$ glasses by X-ray diffraction and B-11 MAS NMR techniques. J Am Ceram Soc. 2000;83(10):2543–8.

70. Martin V, Wood B, Werner-Zwanziger U, Zwanziger JW. Structural aspects of the photoelastic response in lead borate glasses. J Non Cryst Solids. 2011;357(10):2120–5.

71. Shaw JL, Werner-Zwanziger U, Zwanziger JW. Correlation of lead borate glass structure with photoelastic response. Phys Chem Glasses B. 2006; 47(4): 513–7.

72. Leventhal L, Bray AJ. Nuclear magnetic resonance investigations of compounds and glasses in the systems PbO-B$_2$O$_3$ and PbO-SiO$_2$. Phys Chem Glasses. 1965;6(4):113–25.

73. Alderman OLG. The structure of vitreous binary oxides: silicate, germanate and plumbite networks, PhD thesis, Department of Physics, University of Warwick, 2013. p. 254.

74. Xu Y, Cheng LY, Zhou GP, Wang YL. Lead germanium oxide. Acta Crystallogr E. 2006;62:I135-7.

75. Nozik YZ, Maksimov BA, Fykin LE, Dudarev VY, Garashina LS, Gabrielyan VT. Neutron-diffraction study of lead germanate PbGeO$_3$. J Struct Chem+. 1978;19(4):628–30.

76. Kasymova SS. Some properties of glasses in the system RO (SrO, BaO)-GeO$_2$ (in Russian). Doklady Akademii Nauk UzSSR. 1982;1:36–8.

77. Shelby JE. Properties and morphology of barium germanate glasses. J Am Ceram Soc. 1984;67(8):557–60.

78. Inaba S, Oda S, Morinaga K. Equation for estimating the thermal diffusivity, specific heat and thermal conductivity of oxide glasses. J Jpn I Met. 2001;65(8):680–7.

79. Pernice P, Aronne A, Catauro M, Marotta A. Glass transition temperature and devitrification study of barium germanate glasses. J Non-Cryst Solids. 1997;210(1):23–31.

80. Avalos CE, Walder BJ, Viger-Gravel J, Magrez A, Emsley L. Chemical exchange at the ferroelectric phase transition of lead germanate revealed by solid state 207 Pb nuclear magnetic resonance. Phys Chem Chem Phys. 2019;21(3):1100–9.

81. Barney ER, Hannon AC, Holland D, Winslow D, Rijal B, Affatigato M, et al. Structural studies of lead aluminate glasses. J Non-Cryst Solids. 2007;353(18-21):1741–7.

82. Hannon AC, Parker JM, Vessal B. Neutron diffraction analysis of the atomic short range order in lead gallate glasses. J Non-Cryst Solids. 1998;232:51–8.

83. Hannon AC, Parker JM, Vessal B. The effect of composition in lead gallate glasses: A structural study. J Non-Cryst Solids. 1996;196:187–92.

84. Dickinson RG, Friauf JB. The crystal structure of tetragonal lead monoxide. J Am Chem Soc. 1924;46:2457–63.

85. Hill RJ. Refinement of the structure of orthorhombic Pbo (Massicot) by rietveld analysis of neutron powder diffraction data. Acta Crystallogr C. 1985;41(Sep):1281–4.

86. Newnham RE, Wolfe RW, Darlington CNW. Prototype structure of $Pb_5Ge_3O_{11}$. J Solid State Chem. 1973;6(3):378–83.

87. Kay MI, Newnham RE, Wolfe RW. Crystal-structure of ferroelectric phase of $Pb_5Ge_3O_{11}$. Ferroelectrics. 1975;9(1-2):1–6.

88. Iwata Y. Neutron-diffraction study of structure of paraelectric phase of $Pb_5Ge_3O_{11}$. J Phys Soc Jpn. 1977;43(3):961–7.

89. Kato K. Crystal-structure of pentalead(II) germanate trioxide. Acta Crystallogr B. 1979;35(Apr):795–7.

90. Otto HH. Crystal-structure of ferroic compound $Pb_3(O/GeO_4)$. Z Kristallogr. 1979;149(3-4):227–40.

91. Kato K, Hirota K, Kanke Y, Sato A, Ohsumi K, Takase T, et al. Crystal-structure of lead germanate $Pb_{11}Ge_3O_{17}$. Z Kristallogr. 1995;210(3):188–94.

92. Baikie T, Pramana SS, Ferraris C, Huang YZ, Kendrick E, Knight KS, et al. Polysomatic apatites. Acta Crystallogr B. 2010;66:1–16.

SUPPORTING INFORMATION

Additional supporting information may be found in the online version of the article at the publisher's website.